MithraREM

Technical notice

Propagation models description

Validation of the computations

EN-DSC/ECE 13.27,28,32.C

July - November 2013, May 2014, March 2015, August 2015, February 2017, October 2024

rev. 7545

N. Noé
F. Gaudaire
J. Martin

CSTB
le futur en construction

October 18, 2024

Contents

List of Figures

List of Tables

Part I

Technical notice

Chapter 1

Introduction

MithraREM is a computation software for the simulation of electromagnetic waves in outdoor environments, especially urban areas.

The overall dimensions of the geometrical models to be handled by MithraREM (a city district, that is to say several squared kilometers) prevent from using exact numerical methods (such as Boundary Elements Method or Finite Difference Time Domain). As a consequence MithraREM is based upon asymptotic methods, as in geometrical optics, where wave propagation is modeled with "rays". Rays are flow lines perpendicular to wavefront (figure 1).

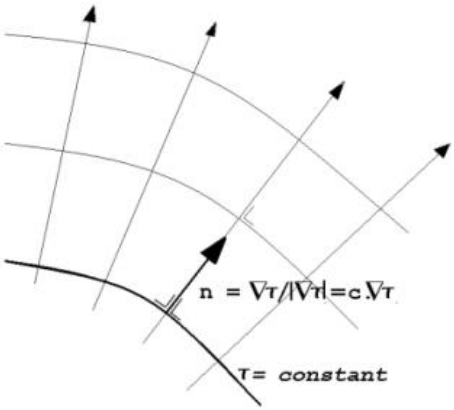

Figure 1.1: Wavefront and rays

These rays are propagated from emitters according to Fermat's principle of least time. Reflection, transmission and diffraction laws are deducted from this principle and applied to the propagated rays.

Consequently a MithraREM computation is made of two steps: a geometrical step (the computation of paths between emitters and receivers) and a physical step (the computation of electric field associated to theses paths). These two steps are totally independent and are done simultaneously within MithraREM: each path found by the geometrical computation is used by the physical computation, and the final result is the electric field at receivers positions. Then the paths are discarded as soon as they have been used. Nevertheless the software allows to display computed paths for isolated receivers in order to check results.

Asymptotic methods are reliable as long as geometry details are rougher than a few wavelengths. In the area of concern (mobile telephony, Wi-Fi, ...), wavelength are lower than 30cm hence geometrical details must be greater than a meter. This constraint is usually fulfilled with GIS originating models.

Chapter 2

Computation model

Because of the large scale of geometrical models (city-like), it is out of the question to predict electromagnetic waves propagation using a direct 3D ray-tracing computation handling large enough propagation distance, all of the buildings in the city-district, and high enough order of reflection and diffraction to correctly compute electromagnetic field levels.

Furthermore GIS models are mainly 2.5D data, that is to say a numerical model where ground altitude $z = f(x, y)$ is a function of horizontal location, and where buildings are defined by their ground shape and their height.

That is why the geometrical computation is based upon a 2.5D model. As a matter of fact this approach allows to reach very low computation times (compared to full 3D computation), with a large number of buildings and interactions (reflections and diffractions) taken into account. This 2.5D approach is the one usually used in noise mapping for instance.

It is very important to notice that even with a 2.5D model, the electric field computation is performed in 3D. Hence 2.5D is only a limitation for the kind of geometries that can be handled. This 2.5D model does not require flat buildings roofs, but does not allow ground overlapping (such as a tunnel) [1]. Examples of what can be done or not with 2.5D models are displayed on figure 2.1.

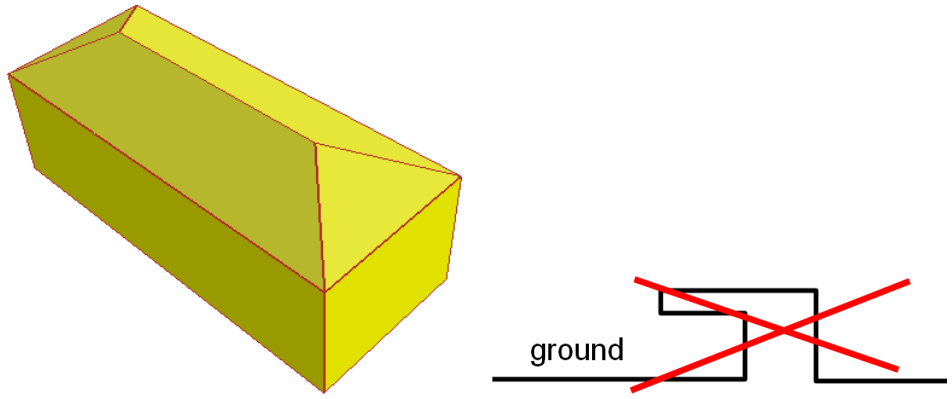

valid 2.5D geometry invalid 2.5D geometry

Figure 2.1: 2.5D vs. 3D geometry

[1] CSTB does provide equivalent softwares for real 3D computations that can be used in this case.

Chapter 3

Geometrical computation

The goal of the geometrical computation is to find all paths between identified sets of emitters (as points) and receivers (as points), taking into account reflections and diffractions by the geometry. As said earlier the geometrical computation is based upon a 2.5D geometrical model. First computations are performed in 2D (in the horizontal xy plane) then are transformed into 3D results.

3.1 From 3D to 2D

3.1.1 Reflection

Reflections on surfaces are considered as specular ("mirror" reflection), according to Fermat's principle. Because of the 2.5D geometrical model these reflections can only exist on vertical walls (front sides of buildings).

A geometrical property is that a specular 3D reflection (on a vertical wall) is still specular in the 2D plane, replacing the the wall by a projected segment. To switch back from 2D into 3D one just has to compute the reflection height on the wall (see figure 3.1), taking into account emitter and receiver heights, using an image-source technique.

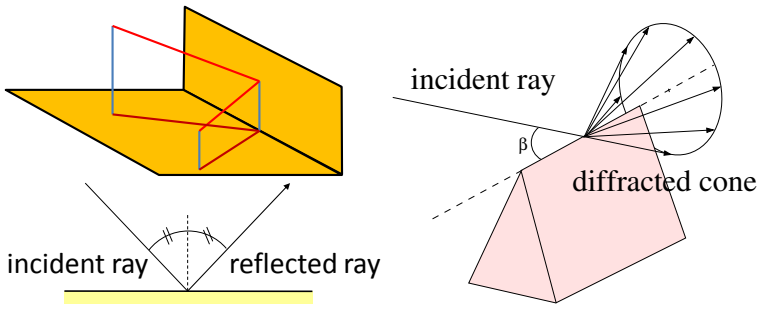

Figure 3.1: Reflection and diffraction

3.1.2 Diffraction

Diffraction is taken into account using Geometrical Theory of Diffraction (GTD) and Unified Theory of Diffraction (UTD). This theory encompasses Fermat's principle as an incident ray on an edge with an angle β is diffracted into a cone of diffraction rays having the same angle β with the edge (see figure 3.1).

Because of the 2.5D geometrical model there only are two kinds of diffracting edges: vertical edges (vertical edges of buildings) and almost horizontal edges (on rooftops, on ground, ...).

A diffracted path by an horizontal edge between an emitter and a receiver is almost a straight line in the 2D plane because the propagation distances are greater than the buildings heights. As a consequence a straight 2D path over a building could represent this kind of diffraction (see figure 3.2).

As far as vertical edges are concerned they are projected onto a point than itself becomes a secondary order emitter (see figure 3.2).

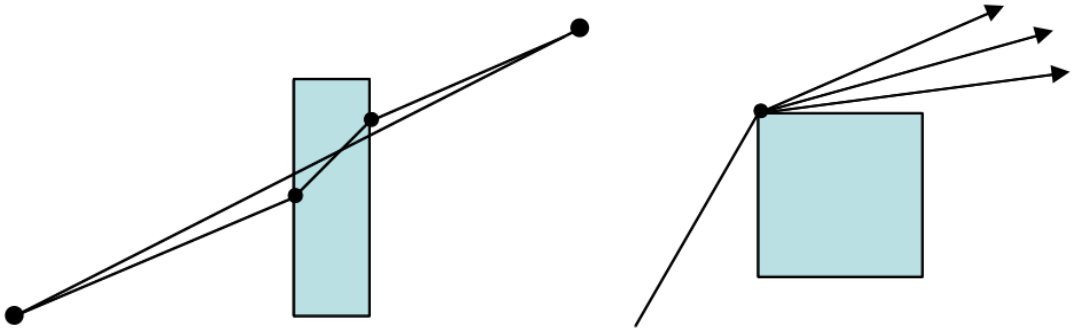

horizontal edges: almost straight lines vertical edges: secondary point sources

Figure 3.2: Diffraction on a 2.5D model (top views)

3.2 Geometrical computation in 2D

The 2D geometrical computation traces 360 degrees wide beams around emitter points. A beam is then an angular sector. These beams are clipped by the intersected geometry (in 2D geometry is made of segments, created by ground and buildings). These beams are both geometrically transmitted (in a straight way) and reflected (in a specular way) by encountered segments of buildings. Beam tracing is illustrated on figure 3.3.

When a beam reaches a vertical diffraction point, a secondary order point source is created, and the process starts again from this new emitter.

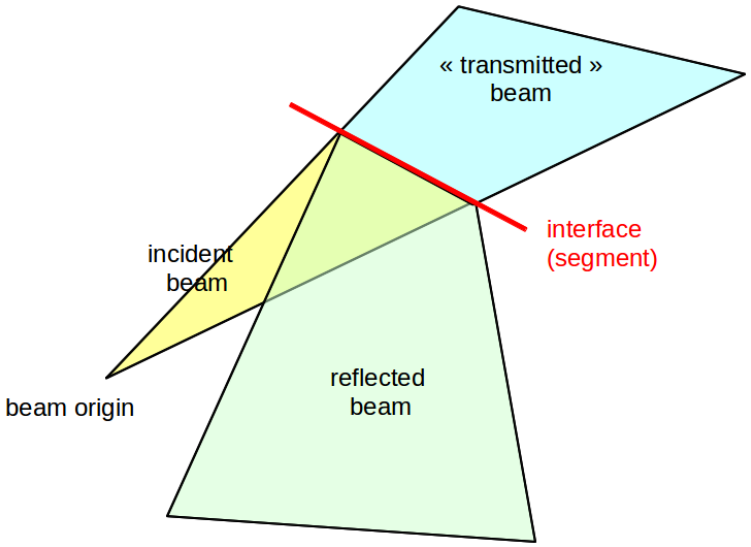

Figure 3.3: Reflection and diffraction

The beam clipping is performed until a maximum propagation distance is reached or a maximum order of reflection or vertical diffraction is reached. These are the three main parameters to configure the geometrical computation.

Once beams are built receivers are located inside them and exact 2D paths are generated using image-source technique, as illustrated on figure 3.4.

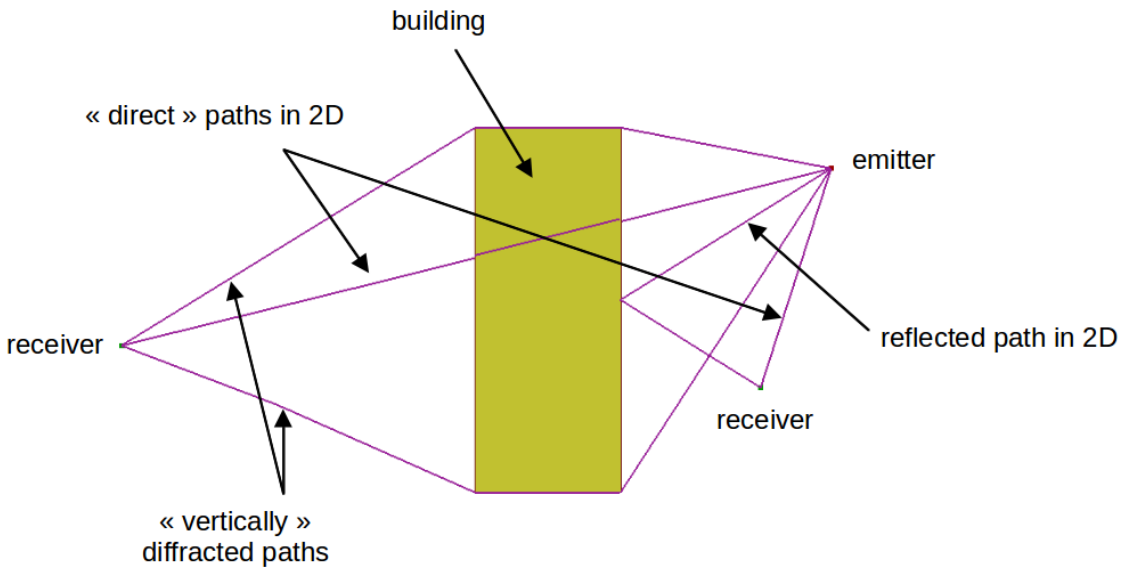

Figure 3.4: 2D paths computation

3.3 Geometrical computation in 3D

The principle of 3D computation is to construct 3D paths associated to each 2D path found. The main 3D path is found using convex hull method, taking into account emitter and receiver heights (see figure 3.5). In the same time the heights of the path on the obstacles (for reflection and diffraction on vertical edges) is found. As a consequence the 3D path might not exist (reflection higher than the wall for example).

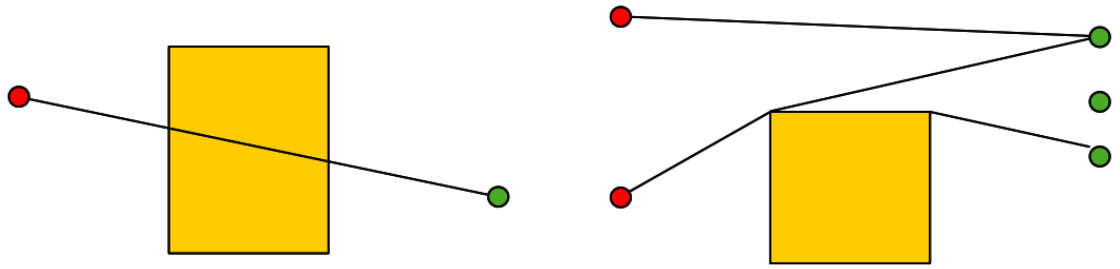

in the horizontal plane xy in the vertical cut-plane dz

Figure 3.5: From 2D path to 3D path

Ground reflection is also added to the the contributions. This reflection is computed in the vertical cut-plane of the "unfolded" path along its propagation direction. Diffracted paths in the illuminated region can also be added, as these paths enhance the electric field continuity in transition regions.

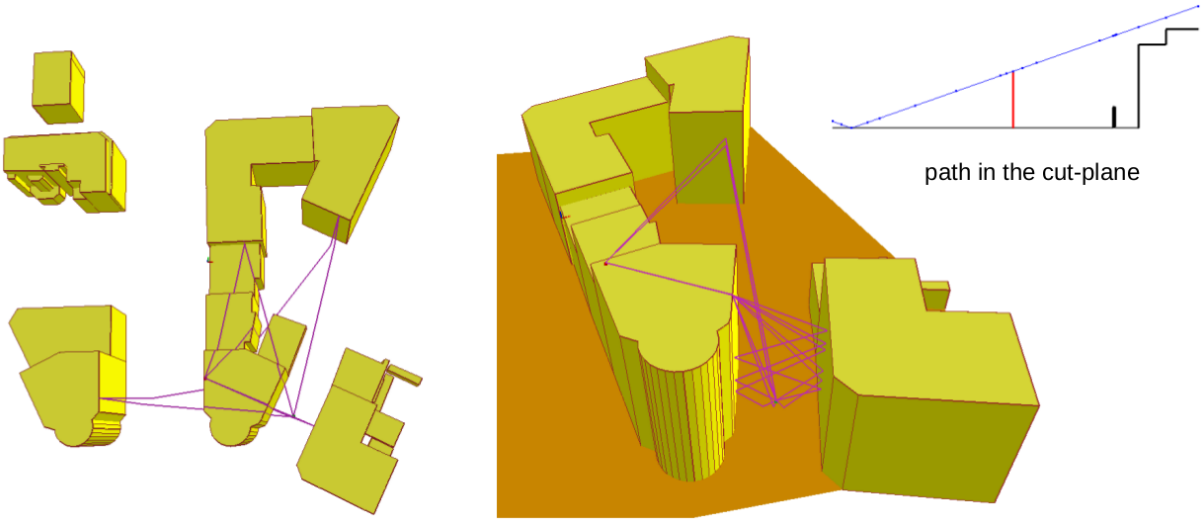

Figure 3.6: 2D paths and corresponding 3D paths

As far as diffraction by horizontal edges is concerned the exact position of the diffraction point must also be computed in order to fulfill GTD. This leads to slightly move the original point on the diffraction edge so as to have identical incident and diffracted angles in 3D. This is illustrated on figure 3.7.

When several emitters share the same 2D position (for instance three antennas with three different azimuths on the same mast) or where several receivers share the same 2D position (receivers in front of a

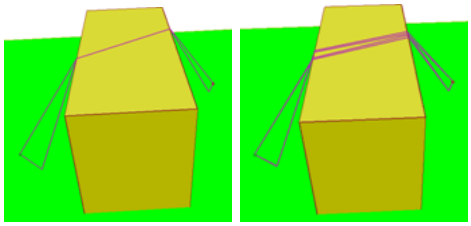

Figure 3.7: Exact GTD computation (left without GTD, right with GTD)

building, one at each floor) the computation will only consider a single 2D emitter and a single 2D receiver. It it only when computing the 3D paths (far less time consuming the computing the 2D paths) that the exact heights are taken into account.

Chapter 4

Electromagnetic computation

4.1 Introduction

For each computed 3D path the transfer function from the emitter to the receiver is computed. This transfer function takes into account the directivity of the emitter, the reflection and diffraction coefficients (depending on the materials hit on the path) and the geometrical path loss. This transfer function computes a complex 3D vector of electric field, depending on frequency (and phase) and accounting for polarization (in the magnetic plane and in the electric plane).

4.2 Free field propagation

From Maxwell's equations and hypothesis of asymptotic methods are deducted phase propagation law and energy conservation law. As a consequence the propagation of the electric field between two points P_0 and P in beam of rays depends on the arc length s between P_0 and P and the caustic distance ρ_1 and ρ_2 of the beam:

$$\vec{E}(P) = \vec{E}(P_0)\sqrt{\frac{\rho_1\rho_2}{(\rho_1+s)(\rho_2+s)}}e^{-jks} \text{ (V/m)} \tag{4.1}$$

In case of spherical waves emitted by a point source (and with reflections on planar surfaces) the beam of rays is a pyramid and then $\rho_1 = \rho_2 = s_0$, where s_0 is the distance from the emitter to the receiver. For a point source of power W in watt we have:

$$\left|\vec{E}(P)\right| = \sqrt{\frac{\mu_0 cW}{4\pi}}\frac{1}{s_0}e^{-jks_0} = \frac{\sqrt{30W}}{s_0}e^{-jks_0} \text{ (V/m)} \tag{4.2}$$

4.3 Electromagnetic waves polarization

An electromagnetic wave is polarized and the polarization is propagated along a path. The polarization is decomposed in the ray local coordinate system. The incident plane is defined as the plane that contains the incident ray and the normal at the interaction point. The component of the electric field that is perpendicular to the incident plane is called TE (for transverse-electric) or perpendicular component. The component of the electric field that lies in the incident plane is called TM (for transverse-magnetic) or parallel component. Far from the emitter we have planar waves hence there is no component along the direction of the ray. The polarization of the waves is illustrated on figure 4.1 and can be written as:

$$\vec{E} = E_{\parallel}\vec{u}_{\parallel} + E_{\perp}\vec{u}_{\perp} \tag{4.3}$$

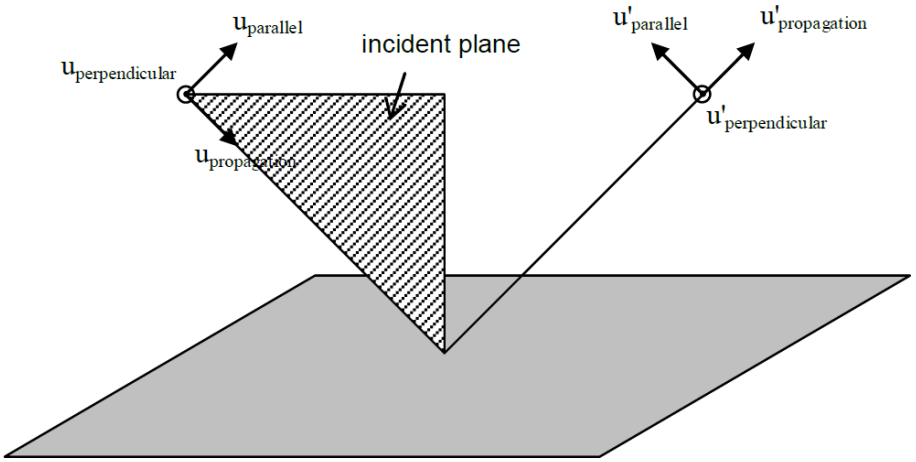

Figure 4.1: Polarization of electromagnetic waves

4.4 Reflection of electromagnetic waves

Materials are supposed to be non-magnetic ($\mu = \mu_0 = 4\pi \cdot 10^{-7}$ H/m), homogeneous and isotropic. The complex dielectric permittivity is defined as: $\bar{\epsilon} = \bar{\epsilon_r} \cdot \epsilon_0$. ϵ_r is the relative complex permittivity and $\epsilon_0 = 8.85 \cdot 10^{-12}$.

The complex relative permittivity is defined as:

$$\bar{\epsilon_r} = \epsilon' - j\epsilon'' = \epsilon' - j\frac{\sigma}{2\pi f \epsilon_0} \tag{4.4}$$

With f the frequency (in Hz) and σ the conductivity (in S/m). Each material is then defined by the real part of its relative permittivity (ϵ', no dimension) and its conductivity σ (in Siemens / meter). The impedance of the material is defined as:

$$Z = \sqrt{\frac{\mu_0}{\bar{\epsilon}}} = Z_0 \cdot Z_r = Z_0 \cdot \frac{1}{\sqrt{\bar{\epsilon_r}}} \tag{4.5}$$

With Z_r the relative impedance that is the ratio of the material impedance at the interface and the void impedance $Z_0 = \sqrt{\mu_0/\epsilon_0} = 120\pi$. The relative admittance is the inverse of the relative impedance: $Y_r = 1/Z_r = \sqrt{\bar{\epsilon_r}}$.

The hypothesis of local reaction (in ray theory) justifies the existence of a reflection coefficient that relies reflected field to incident field. These reflections coefficients differ for TM and TE polarized waves. They are defined as:

$$R_{\parallel} = \frac{Y^2\cos\theta - \sqrt{Y^2 - \sin^2\theta}}{Y^2\cos\theta + \sqrt{Y^2 - \sin^2\theta}} = \frac{\bar{\epsilon_r}\cos\theta - \sqrt{\bar{\epsilon_r} - \sin^2\theta}}{\bar{\epsilon_r}\cos\theta + \sqrt{\bar{\epsilon_r} - \sin^2\theta}} \tag{4.6}$$

$$R_{\perp} = \frac{\cos\theta - \sqrt{Y^2 - \sin^2\theta}}{\cos\theta + \sqrt{Y^2 - \sin^2\theta}} = \frac{\cos\theta - \sqrt{\bar{\epsilon_r} - \sin^2\theta}}{\cos\theta + \sqrt{\bar{\epsilon_r} - \sin^2\theta}} \tag{4.7}$$

With θ the incident angle on the surface ($\theta = 0$ for normal incidence). In case of a PEC (perfect electric conductor) material (i.e. metallic material), σ is infinite and the $R_{\parallel} = -1$ and $R_{\perp} = 1$.

4.5 Transmission of electromagnetic waves

An attenuation coefficient can be defined for a given material. It is usually a dB value and can be independent from the frequency. It is used in order to compute electric level on the inner side of buildings frontages. This coefficient is a loss in diffuse field (averaged loss over all incident directions and polarisations, measured in coupled reverberant rooms).

4.6 Diffraction of electromagnetic waves

As seen earlier diffraction is computed with Uniform Theory of Diffraction (UTD). Like reflection, incident plane (defined by incident ray on the diffracting edge and tangent of the edge at the diffraction point) is used to compute polarized components of electric field. The diffraction coefficients take into account the aperture of the wedge, the material and the incident angles. A dedicated path-loss is also computed for diffracted waves. All of these expressions are far too complex to be detailed here. For basics on UTD please refer to Kouyoumjian and Pathak's seminal article[1]. A lot of development has also been conducted through the years to improve these diffraction coefficients.

4.7 Full computation

All transfer functions (for each 3D path) are added (with phase) in order to compute the full transfer function from an emitter to a receiver. These emitter-to-receiver transfer functions allow to switch on or off dynamically emitters while viewing results.

On a practical point of view, electric fields from different emitters reaching a single emitter are added incoherently, in order to achieve a scalar electric field in V/m. Nevertheless while comparing simulation to measurement it might be useful to know the 3D components of the field.

4.8 Antennas

Antennas can be modeled with a far-field radiation diagram (a full 3D diagram or a pair of horizontal and vertical 2D diagrams). Antennas can also be modeled with a set of dipoles (each dipole having a relative position to the antenna reference position) with a diagram per dipole of TM and TE polarized radiation. Both models are equivalent in far field (Fraunhoffer's area) but the latter choice allows better electric field accuracy in near-field (Fresnel's area farther than Rayleigh's area).

[1] R.G. Kouyoumjian, P.H. Pathak "A Uniform Geometrical Theory of Diffraction for an Edge in a Perfectly Conducting Surface", Proc. IEEE, Vol. 62, 1974

Bibliography

[1] "Measurement Method of Electromagnetic Transmission Loss of Building Components Using Two Reverberation Chambers", B. Foulonneau, F. Gaudaire, Y. Gabillet - Electronics Letters, Vol. 32/23, November 1996

[2] "Propagation radio dans le bâtiment : une nouvelle approche", F. Gaudaire, Y. Gabillet - Revue de l'Electricité et de l'Electronique, N. 11, Décembre 1997

[3] "A Mixed Ray Launching / Tracing Method for Full 3-D UHF Propagation Modelling and Comparison with Wideband Measurements", J-P. Rossi, Y. Gabillet - IEEE transactions on Antennas and Propagation, Vol. 50/4, April 2002

[4] "Simulation of the Indoor Propagation of a 60 GHz Electromagnetic Wave with a Time-Dependant Radiosity Algorithm", G. Rougeron, F. Gaudaire, Y. Gabillet, K. Bouatouch - Computer and Graphics, Vol. 26, 2002

[5] "Integral Formulation for Field Prediction in Complex Scenes", E. Conil, F. Gaudaire, J-C. Bolomey - European Conference on Propagation and Systems, Brest, France, 2005

[6] "A Tool for Far Field's Prediction Extended to Include Effects of Near Field's Objects", E. Conil, F.Gaudaire, J.Ch. Bolomey - Proc. of IEEE International Symposium on Microwave, Antenna, Propagation and EMC Technologies for Wireless Communications, Beijing, Chine, 2005

[7] "A General Ray-Tracing Solution to Reflection on Curved Surfaces and Diffraction by their Bounding Edges", N. Noé, F. Gaudaire - ICTCA conference, Dresden, Germany, 2009

[8] "Using Asymptotic Methods to Compute Diffracted Pressure by Curved Surfaces", M. Vermet, N. Noé - ICTCA conference, Dresden, Germany, 2009

[9] "Simulation de la propagation des ondes électromagnétiques en milieu urbain : applications et perspectives", N. Noé et F. Gaudaire - Journées "dosimétrie des ondes radiofréquences dans les projets ANR", Telecom Paris Tech, 9&10 novembre 2009

[10] "Reflection on Curved Surfaces in a 2.5D Ray-Tracing Method for Electromagnetic Waves Exposure Prediction in Urban Areas", N. Noé, F. Gaudaire - proceedings of the XXX$^{\text{th}}$ URSI General Assembly, Istanbul, Turkey, 2011

[11] "Méthode d'analyse de l'exposition des populations et de la couverture radio des réseaux de téléphonie mobile GMS et UMTS" F. Gaudaire, N. Noé, J-B. Dufour, R. De Sèze et al - Revue de l'Electricité et de l'Electronique, N. 5, Décembre 2012

[12] "Estimating and Reducing Uncertainties in Ray-Tracing Techniques for Electromagnetic Field Exposure in Urban Areas" N. Noé, F. Gaudaire, M. Diarra Bousso Lo, Proc. of IEEE Conference on Antennas and Propagation in Wireless Communications, Torino, 2013

Part II

Propagation models description

Chapter 5

Introduction

MithraREM deterministic propagation models are :

- CSTB2009.1
- CSTB2009.2
- CSTB2013
- CSTB2013-INDOOR
- CSTB2016
- CSTB2016-INDOOR

There also exist heuristic and hybrid models :

- HATA Ex
- HATA Ex + Fresnel

5.1 Propagation model CSTB2009

This is the original MithraREM propagation model, used in MithraREM $\leq$ 1.5.X.

5.2 Propagation model CSTB2013

This is the new MithraREM propagation model, used in MithraREM $\geq$ 1.6. This model improves the original model by reducing uncertainties to input data and computation parameters. Some of the improvements were induced by feedback from end-users and some of the improvements come from CSTB work on research projects and practical applications.

5.3 Propagation model CSTB2013-INDOOR

This is a newly introduction propagation model, starting with MithraREM 1.7. It is dedicated to indoor exposure computation (just behind the exterior wall) and is identical to CSTB2013 model for outdoor exposure.

5.4 Propagation models CSTB2016 and CSTB2016-INDOOR

These two models are an update of CSTB2013 and CSTB2013-INDOOR models, with an improved search of high levels in case of direct visibility of an antenna.

5.5 Propagation model HATA Ex

This is extended Hata propagation model. This kind of heuristic model only relies on heights of emitter and receiver, horizontal propagation distance and environment type.

5.6 Propagation model HATA Ex + Fresnel

This is a hybrid propagation model, using both a geometrical computation of the first Fresnel ellipsoid clearance for point-to-point link estimation, and the extended Hata model.

Chapter 6

Description of propagation model CSTB2013

6.1 Introduction

The propagation model CSTB2013 is an evolution of the propagation model CSTB2009. This evolution make it more relevant in electric field computation in an urban environment.

This evolution does not challenge results computed with earlier model, but gives more stable results and improves results quality in some areas.

Most of the modifications aimed at improving stability of simulation results, in order to lower dependency to slight changes in input data, computation parameters, ...

We present here all the changes between the CSTB2009 propagation model and the CSTB2013 propagation model.

6.2 Order of reflection

In the CSTB2009 model the parameter "order of reflection" included both reflections on vertical walls of buildings and on ground. As a consequence a receiver in the front of a building received potentially less reflected waves than the same receiver in free field. As a matter of fact an order of reflection was "consumed" to take into account the reflection on the wall where the receiver lies.

In order to be coherent between a frontage map computation and a ground map computation, the frontage reflection (for a receiver on that frontage) is systematically added, independently from the parameter "order of reflection". For the same reasons, the same change is applied to ground reflection. Hence the the parameter "order of reflection" now stands only for free-field reflection on vertical walls.

Differences between CSTB2009 and CSTB2013 propagation models are illustrated on the example of figure 6.1.

With an order of reflection equal to one, 4 paths are found for a receiver in frontage of building B with propagation model CSTB2009: direct path, reflected path on the ground, reflected path by building A, reflected path by building B. With propagation model CSTB2013 8 paths are found: the previous ones, reflected path by building A and ground, reflected path by building B and ground, reflected path by buildings A and B, reflected path by building A, B and ground.

This change ensures a faster convergence to the physical solution (with the same order of reflection, hence the same computation time, more paths are taken into account) and a better stability of the results to local variations of the geometrical solution (appearance or disappearance of a reflection on a frontage does not modify path finding of ground reflections or reflections on the frontage where the receiver lies).

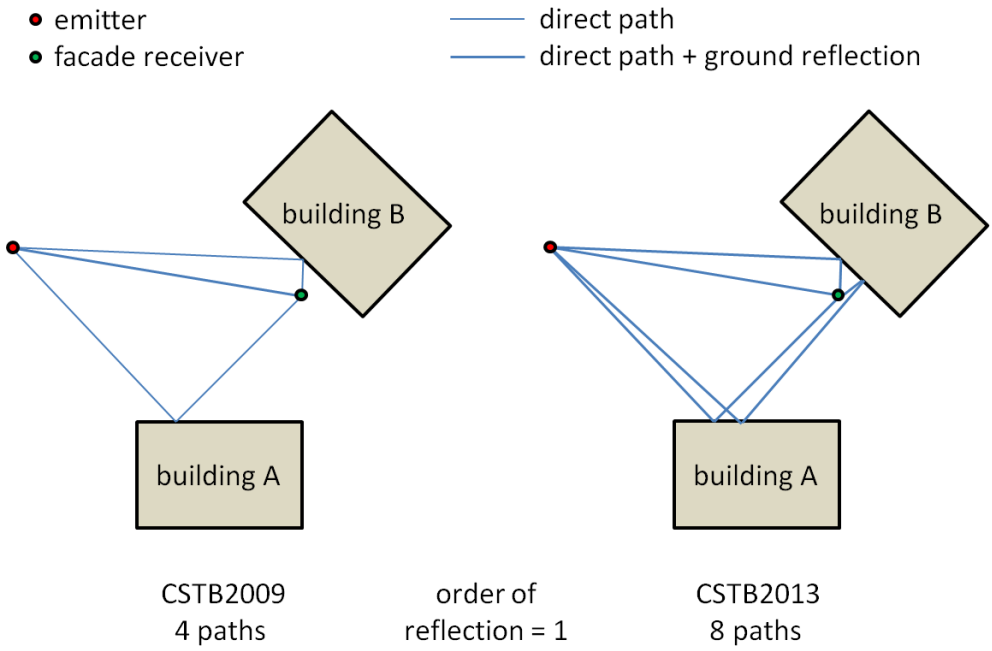

Figure 6.1: Meaning of the parameter "order of reflection"

6.3 Ground reflection

6.3.1 Ground reflection on a 3D path

As seen earlier, one and only one ground reflection (when it exists) is added to each path or part of path connecting transmitter, diffraction points and receiver, whatever the order of reflection is.

6.3.2 Cubic interpolation of the ground

The ground is made of a triangular mesh, generated by constraints (terrain points, terrain lines, ...). Consequently there are slope breaks at each edge of a triangle. When ground reflection is generated using image source method (as in CSTB2009 propagation model), it might not exist since the ground discontinuity introduces shadow areas. This problem is illustrated on figure 6.2. With cubic interpolation (on the left) ground reflections appear or disappear randomly, hence leading to an artificial discontinuity of the solution (and the electric field). With cubic interpolation (on the right) the solution is naturally continuous (geometrically and physically).

This solution improves electric field continuity over the ground. Furthermore it reduces dependency to the ground resolution (using loose or dense set of points will lead to rather similar results) [1].

[1] This is a rather classic problem of ray methods. For the same problem with reflection on curved surfaces see: N. Noé, F. Gaudaire, P. Jean, M. Vermet, "A general Ray-Tracing Solution to Reflection on Curved Surfaces and Diffraction by their Bounding Edges", in Proceedings of the 9th ICTCA, Dresden, Germany, 2009 and N. Noé, F. Gaudaire, "Reflection on Curved Surfaces in a 2.5D Ray-Tracing Method for Electromagnetic Waves Exposure Prediction in Urban Areas" in Proceedings of URSI General Assembly, Istanbul, Turkey, 2011

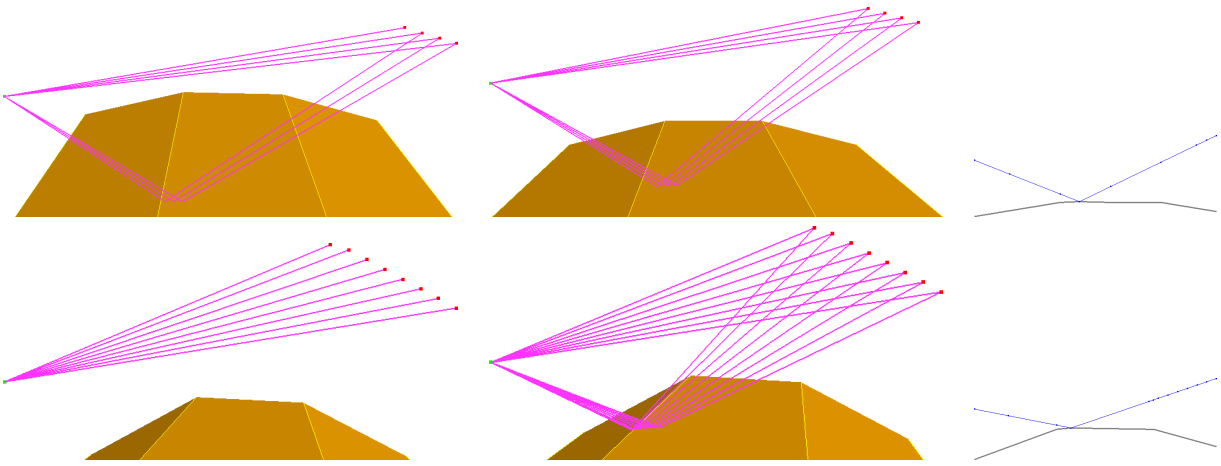

CSTB2009 propagation model: ground reflections do not always exist on the meshed ground. Furthermore the effect depends on the ground definition precision (finer on top, coarser on bottom).

CSTB2013 propagation model: ground reflections continuously exist on the cubic interpolated ground, and do no more depend on the precision of the ground definition.

reflection point on the cubic interpolation for one of the ground reflected path.

Figure 6.2: Cubic interpolation of the ground

6.4 Receiver on a frontage

6.4.1 Reflection on a frontage (for a receiver on a frontage)

As seen earlier, in case of a frontage receiver, the reflection on the frontage itself is always added, whatever the order of reflection is.

6.4.2 Computation of the electric field on the frontage

In case of a receiver on the frontage of a building, the electric field is the addition of the incident waves and the reflected waves by the frontage itself. Interference between incident and reflected waves modify the overall electric field level. These interferences depend on the distance of the receiver from the frontage and on the wavelength. For instance on figure 6.3 (GSM1800 transmitter in front of a building), we get important variations in the electric field on the frontage, depending on the distance of the receiver to the frontage, as shown on figure 6.4).

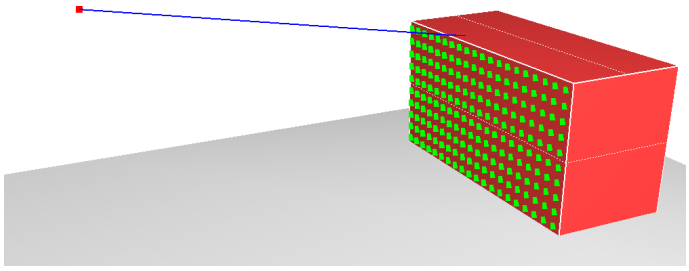

Figure 6.3: A receiver map in front of a building

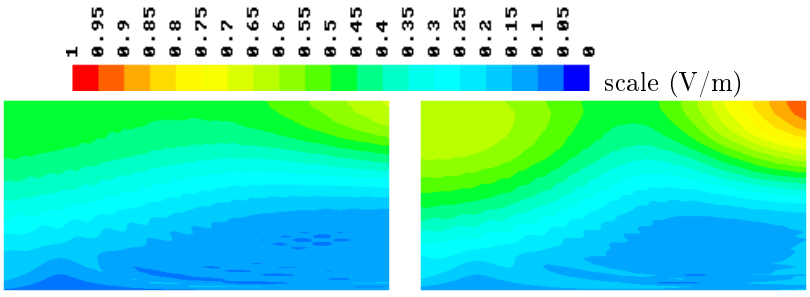

CSTB2009 propag. model: map 10cm from the frontage

CSTB2009 propag. model: map 20cm from the frontage

Figure 6.4: Electric field on the frontage of a building with interferences between direct field and reflected field by the frontage (GSM1800)

On a practical point of the view the reflection on the frontage should take into account the complexity of the frontage (balconies, windows, ...). Since this complexity is not available in the geometrical model, it is more realistic to consider an energetic reflection than a field reflection (the latter accounting for a phenomenon - specular reflection on a planar frontage - very different from the real local behaviour of the waves, especially at short range from the average plane of the real frontage).

Furthermore as is done in measurement and to acknowledge that the distance to the frontage is small (compared to architectural details) it is logical to perform a quadratic averaging of the electric field on a distance at least equal to the wavelength. This choice has been made in the CSTB2013 propagation model and leads to results on figure 6.5.

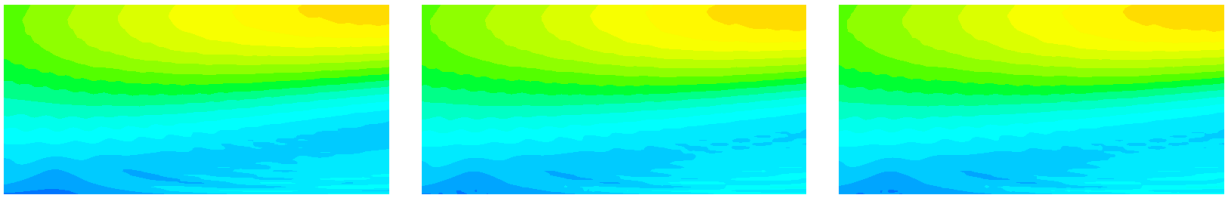

CSTB2009 method: "hand made" quadratic averaging from 1 to 30cm

CSTB2013 method: algorithmic quadratic averaging at 10cm

CSTB2013 method: algorithmic quadratic averaging at 20cm

Figure 6.5: Electric field on the frontage of a building: quadratic addition of incident field and reflected field by the frontage (GSM1800)

The advantage of this solution against the previous one is that the result in almost independent from the distance of the receiver to the frontage, hence reducing uncertainty. Furthermore the quadratic averaging is done algorithmically, not impacting computation time.

6.5 Physical diffraction model

The physical diffraction model used by CSTB2009 method was the one from the uniform theory of diffraction (UTD) of Pathak and Kouyoumjian (P&K). In CSTB2013 method we also use UTD model of Capolino and Albani (C&A). This diffraction model extends the validity range of asymptotic methods in case of creeping waves, whatever the width of the double wedge is.

A practical use is the case of a thin wall (or a parapet) 30cm wide, in GSM900. For three reception points behind the wall, in more or less deeper shadow region, we get the results of figure 6.6.

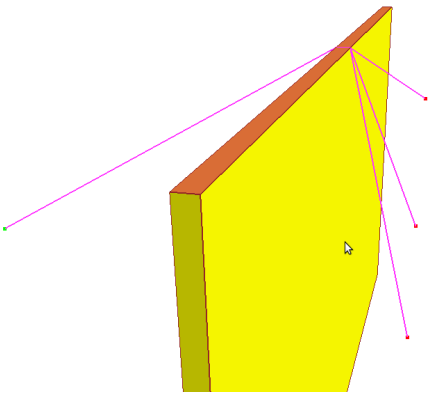

P&K	C&A
0,33 V/m	0,39 V/m
0,14 V/m	0,14 V/m
0,09 V/m	0,09 V/m

Figure 6.6: Comparison between Pathak and Kouyoumjian's (P&K) diffraction model and Capolino and Albani's one (C&A)

The effect of the wall was overestimated with Pathak and Kouyoumjian's model. In case of a wider rooftop, the effect would have been negligible. This is just a margin improvement but it improves physical results in some critical regions.

6.6 Electric field near transmitters

The computation method used in MithraREM software is suited for outdoor exposure level prediction in urban environments, in the far field of each simulated antenna. The method was locally adapted in order to estimate a representative electric field close to the antennas, in the near field area.

6.6.1 Theoretical aspects

An electromagnetic wave does not have the same propagation behaviour in the whole space around an emitter. To model wave propagation in a global environment it is necessary to partition space into different regions. Classically four regions are identified, from the closest to the farthest to the emitting antenna, as illustrated on figure 6.7, where D is the largest "electrical" dimension of the antenna:

- Reactive field region: this "narrow" region is located closer than $\frac{\lambda}{2\pi}$ to the antenna. Wave are evanescent and propagation phenomena are negligible compared with radiative phenomena.
- Rayleigh's region: it is located at distances longer than $\frac{\lambda}{2\pi}$ and shorter than $\frac{D^2}{2\lambda}$. Electromagnetic energy is confined within a cylinder around the radiating aperture. There is very little wave divergence.
- Fresnel's region: this is an intermediate region at distances longer than $\frac{D^2}{2\lambda}$ and shorter than $\frac{2D^2}{\lambda}$. The wave naturally diverges. Associated with Rayleigh's region, these two regions are called the near field (NF) region of the antenna.

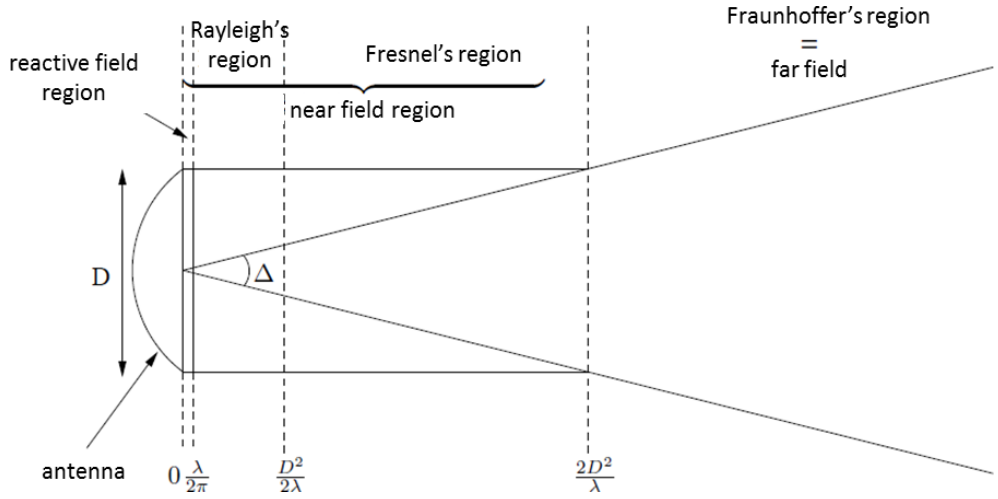

Figure 6.7: Radiation regions around an emitting antenna

- Fraunhoffer's region: it it located beyond $\frac{2D^2}{\lambda}$ and constitutes the so-called far field region of the antenna. The radiated energy lies within a conic beam. In this case, waves are plane waves.

As far as this near field / far field concept is concerned, it should not be considered as a discontinuous frontier, through which propagated wave characteristics would change instantaneously. The given values used in the definition of the propagation regions are informative and can vary. As a matter of facts, considering asymptotic methods, the conditions of usage and validity (as assessed by usage or by comparisons with measurements, ...) go farther than theoretical limits. The results, although altered, are still acceptable. This is a general consideration, whatever the physical domain of application is. For instance, the behaviour in the end of Fresnel's region is very close to the behaviour in the beginning of Fraunhoffer's region.

It is also very important not to confuse the electrical dimension (D) of the antenna with the real world overall dimension (H) of the antenna (in other words, the outer shell). For instance, a base station panel antenna is made of multiple sub-elements, emitters and receivers.

It is also worth mentioning that,in most cases, the electrical dimension of the antenna is proportional to the wavelength (whip, quarter-wave dipole, ...). Hence the frontier between near field and far field can be considered as proportional to the antenna dimension, in a first approach.

The computation method used in MithraREM software is dedicated to the computation of outdoor exposure levels in urban environments, in the far field of each considered antenna. The computation method was locally adapted in order to be able to estimate a representative electric field close to the antennas, in the near field region, considering:

- available data on emitters: a far field diagram of antennas and possible outer shell dimension,
- that the precise description of the environment close to the antennas (geometry and materials) is not available,
- for a number of concerned countries,the definition of mandatory safety perimeters (perimeters that were once determined using precise near field computation methods),
- a statistical approach, each case being a unique one,
- feedback on this near field - far field issue in other fields of physics: acoustics, optics, ...

6.6.2 Methodology

Panel antennas

Panel antennas for mobile telecommunications are made of a set of sub-elements, each forming an emission / reception pair. These sub-elements are placed far enough from one another in order to avoid electromagnetic coupling. In a first approximation, the small dimension of these sub-elements ($D \approx \lambda$) yields far field begin $\frac{2D^2}{\lambda} = 2\lambda$ far from the sub-elements. In the case where the characteristics of these sub-elements are known (and given), it would be possible to simulate the exposure levels in the near field region of the panel antenna (far field region of each sub-element). This type of simulation and its far field equivalent (gain diagram) are illustrated on figure 6.8.

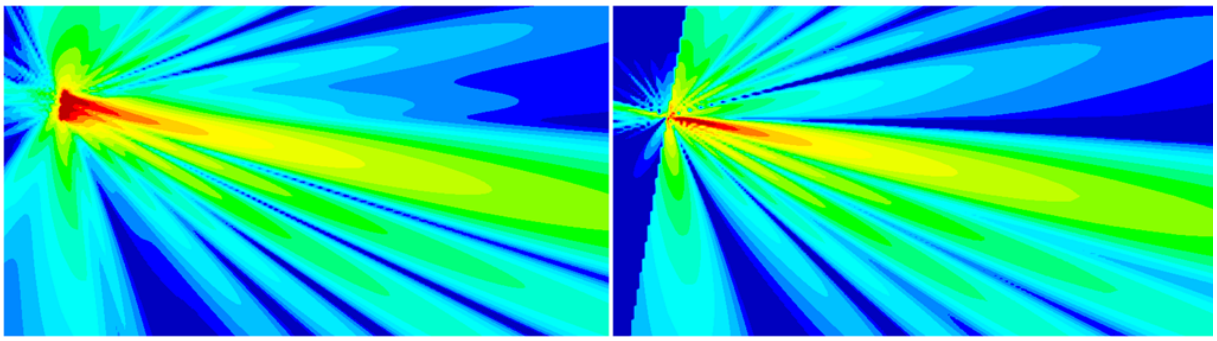

Figure 6.8: Comparison between a so called "near field" model obtained from sub-elements decomposition (left) and an equivalent far field model (right)

Considering the dimension of these antennas, the use of a far field diagram to describe the electric field in the environment is only acceptable far enough from the antenna. This distance is the one where the line source can be replaced by a point source. This is a problem beyond the near field / far field issue since it is a geometrical divergence problem, as illustrated by power density on figure 6.9.

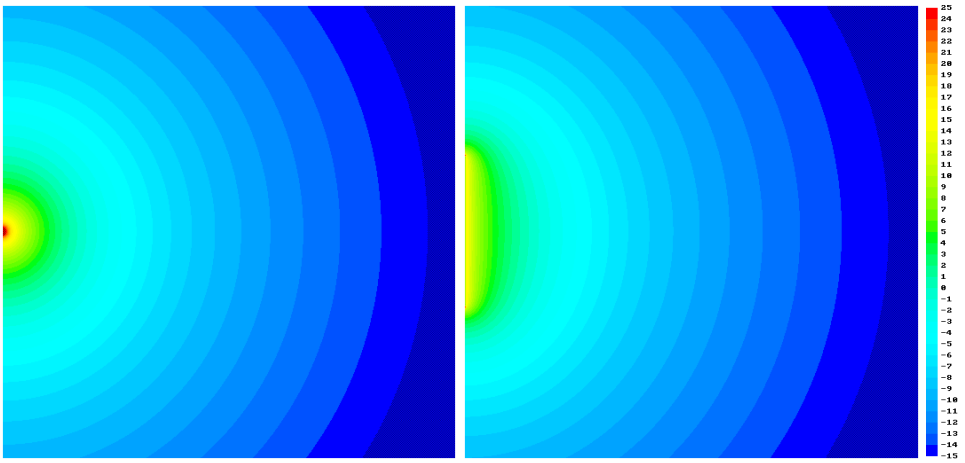

Figure 6.9: Power density (dB) around a 2m line source (left) and a point source (right) with the same radiated power, in a 6x6m region

figure 6.10 illustrates the error in dB between the line source and the point source representations of the geometric divergence as a function of the fraction $K = \frac{r}{H}$. When the distance is longer than $3H$ the error

is below 0.1 dB.

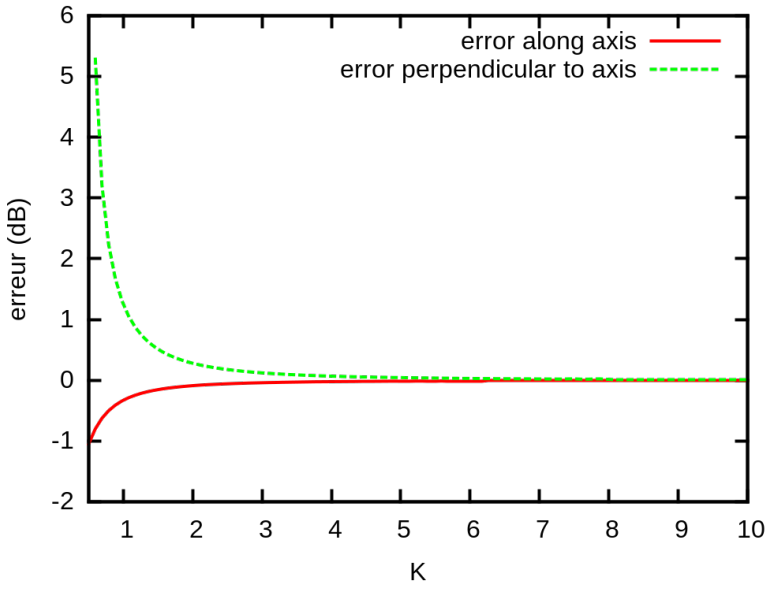

Figure 6.10: Error between the geometric divergence of a line source and the geometric divergence of a point source as a function of the ratio K between distance and source dimension

More generally, the fact that the antenna has a non negligible dimension implies that the emitted lobes are much larger that the lobes of the far field diagram. The electric field near the emitter is then systematically underestimated, even in the far field of the real antenna, as illustrated on figure 6.11.

This fact was confirmed by measurements results close to the antennas, for instance at the outer limit of the safety perimeter, or slightly within the safety perimeter.

This underestimation is more important outside the validity region (i.e. in the near field). however, it would not be relevant to increase the validity region, considering the geometrical problem described above.

Choosing $3H$ as the validity distance then allow one to estimate a field level close to the antennas, even if it is underestimated.

Small dimension antennas

As far as small dimension antennas are concerned (about one wavelength, such as micro-antennas in mobile telecommunications), the far field limit is theoretically reached at a 2λ distance from the antenna. For this kind of antenna, it is theoretically possible to compute the electric field very close to the antenna. However, the uncertainty of the antenna position and of the geometry in the vicinity of the antenna, the distance in the computation method cannot be lower than 1 meter. This 1 meter distance is also in the magnitude of the uncertainty of geometrical data and is coherent with $3H$ distance for lower frequencies of mobile telephony (800 MHz).

Other antennas

Considering the wide range of radio-electric antennas that can be installed in urban environments (panels, dipoles, ...) and considering the available data, i.e. far field gain diagram and sometimes shell dimension, the rule of a validity distance of $D = 3H$ is applied by default. This rule usually underestimates the exposure level close to the antenna. Nevertheless because of high uncertainties in this area (installation, geometry, material, ...) this method is statistically suitable to perform a representative estimation of exposure levels.

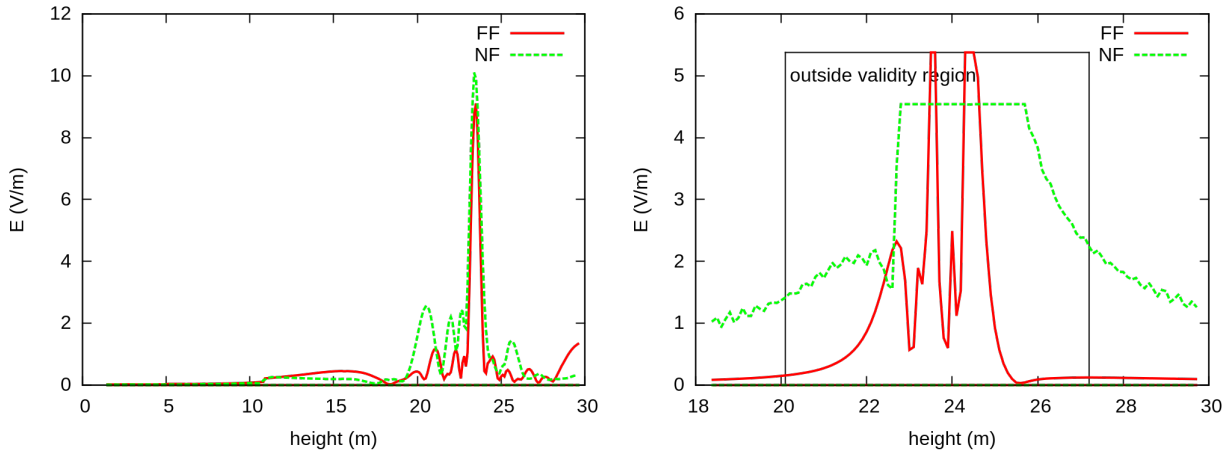

Figure 6.11: Comparison between near field and far field simulations, for a frontage exposure, inside the validity region and outside the validity region

6.6.3 Practical use

The computation method is theoretically valid only in the far field (plane waves). It is then mandatory to set up a distance of validity from the transmitters[2].

However, a slight change in building shape or height can dramatically modify the maximum field, by including or excluding receivers from the validity region. In order to have an stable maximum level in CSTB2013 method it was decided to compute the maximum value of the field (in fact the free field at the limit of the validity region) and to associate this value with the position of the transmitter itself and then to enforce the condition that no level exceeds this maximum value. The value (per transmitter) is computed as:

$$E_{\max} = \frac{\sqrt{30PG}}{d_0}(1+R) \tag{6.1}$$

With:

- P the power of the transmitter (W),
- G the maximal linear gain found for receivers in the line of sight of the transmitter and outside the validity region,
- d_0 the radius of the validity region,
- R the normal reflection coefficient (if the transmitter is on a frontage, 0 otherwise).

Setting this $E_{\max}$ value removes local effects that happen when using receivers on a sphere of radius d_0 around the transmitter. When the height H of the antenna is available, we set $d_0 = 3H$ truncated in the range $[1\,;10]$ [3]. If H is not available, the following values were set:

[2] In CSTB2009 method, receivers out of the validity region were removed from computation results.

[3] according to the French ANFR guide on safety perimeters, one should use 1m as minimal validity distance. Note that the recommended value is 50cm in Belgium, see `http://www.issep.be/files/files/CEM%20et%20telephonie%20mobile.pdf`, paragraph 8.8. MithraREM simulates outdoor electric field, and because of missing other information, indoor field is deduced using a given loss. Within buildings it might not be possible to be as close as 50cm to the emitter (because of wall thickness for example) and the indoor field might be overestimated. The use of a minimal validity distance of 1m takes into account this phenomenon.

$$P < 2W \quad \Rightarrow \quad d_0 = 1 \tag{6.2}$$

$$2W < P < 4W \quad \Rightarrow \quad d_0 = 5^{\frac{P-2}{2}} \tag{6.3}$$

$$4W < P \quad \Rightarrow \quad d_0 = 5 \tag{6.4}$$

These values were obtained from a statistical analysis of existing emitter powers and dimensions over a representative set of cities in France.

6.7 Search for high levels

A receiver on the frontage of building, in line of sight of an antenna and in its main lobe, often means a very high exposure. The maximal exposure is not always the receiver pointed by the azimuth and tilt of the antenna. In fact the free field path loss must be taken into account, and other contributions too. When using simulation software as decision support (computation of the maximal level in an area for instance) the precise computation (position and value) of these "hotspots" is mandatory.

Uncertainties on these hotspots is related to the singular shape of radiation diagrams of transmitters. These diagrams have a highly pinched vertical lobe which -3dB aperture is about 7 degrees. That means that while sliding 7 degrees from the main axis the emitted power is cut by half. For instance the electric field at a receiver 15m away from the transmitter increases or decreases of 2dB when the receiver is moved vertically of 1 meter.

Receivers on frontage of buildings are generated on vertical lines with regular spacing in the CSTB2009 method. Hence results and maximum value is very sensitive to vertical spacing (a computation parameter) and to slight changes in the geometrical model (slight change of altitude or height of a building). In method CSTB2013 an automatic search (during computation, see figure 6.12) of the exact altitude of the most exposed point is performed (without computation overhead). In order not to modify user receivers map, the electric field of the hotspot is assigned to its closest receiver.

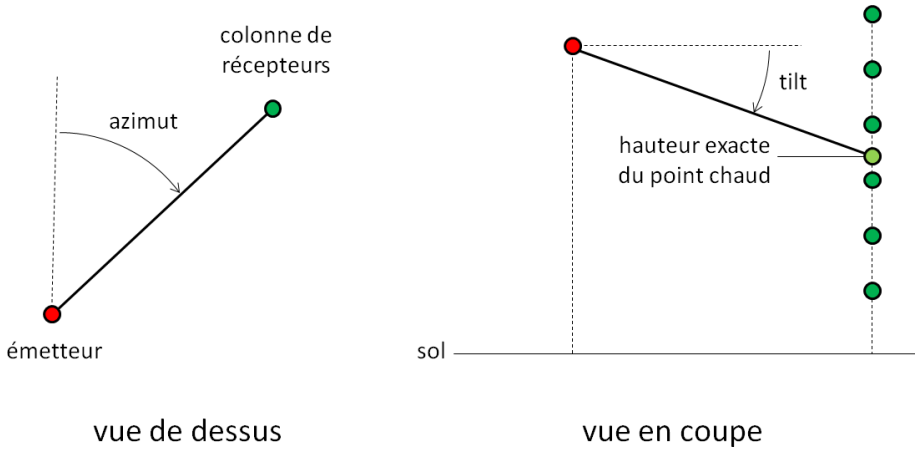

Figure 6.12: hotspot on a vertical line of receivers on a frontage

The efficiency of this evolution can be proved with two computations with two different vertical spacing: one with 9 points and one with 6 points. The test case is illustrated on figure 6.13 and the results in table 6.1.

With CSTB2013 propagation model we get exactly the same maximal electric field (12.77 V/m) in both cases of vertical spacing. Furthermore it appears that the value could be under-estimated with CSTB2009 propagation model, in case of sparse vertical spacing.

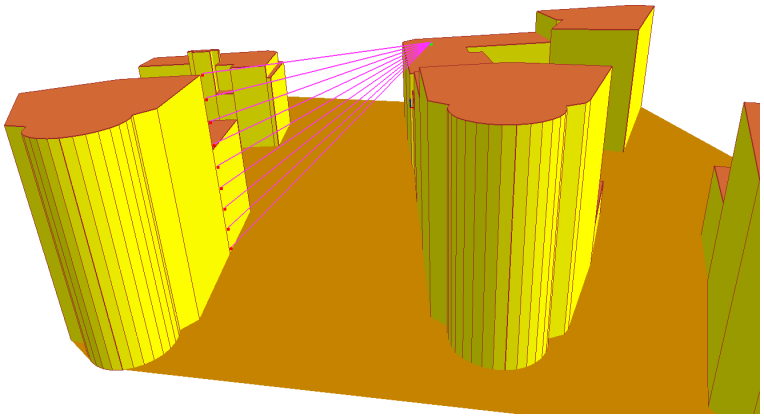

Figure 6.13: Test case for hotspot computation

hauteur	CSTB2009	CSTB2013
1.5	0.62	0.62
4.2	0.42	0.42
6.9	1.55	1.55
9.6	2.37	2.37
12.3	1.42	1.42
14.9	3.12	3.12
17.6	9.32	9.32
20.3	12.71	12.77
23	8.48	8.48

hauteur	CSTB2009	CSTB2013
1.5	0.62	0.62
5.8	1.04	1.04
10.1	2.38	2.38
14.4	2.04	2.04
18.7	11.37	12.77
23	8.48	8.48

Table 6.1: Comparison between CSTB2009 and CSTB2013 methods for hotspot identification

6.8 Spectral sampling

6.8.1 Introduction

Let there be a frequency band $[f_-; f_+]$. This frequency band is sampled for computation on a given number of discrete frequencies f_i, and for each of these frequencies the associated electric field E_i is computed, using a part of the total band power. From there, there are different ways of integrating electric field over the band.

"rectangles-type" integration

For a "rectangles-type" integration the band is sampled into n frequencies $\{f_0, f_1, \dots f_{n-1}\}$, with $f_- < f_0 < f_1 < \dots f_{n-1} < f_+$, as illustrated on figure 6.14. The integration is performed considering the electric field constant and equal to E_i on each interval centered on f_i. The power on each of these intervals is then proportional to the interval width. Hence for $i \in \{0, 1, \dots n-1\}$:

$$P_i = \frac{P}{f_+ - f_-}\left(\frac{f_{i+1} + f_i}{2} - \frac{f_i + f_{i-1}}{2}\right) = \frac{P}{2}\frac{f_{i+1} - f_{i-1}}{f_+ - f_-} \tag{6.5}$$

With $f_{-1} = 2f_- - f_0$ and $f_n = 2f_+ - f_{n-1}$. So we have:

$$\sum_{i=0}^{n-1} P_i = P \text{ and we compute } E^2 = \sum_{i=0}^{n-1} E_i^2 \tag{6.6}$$

the main drawback of this method is that is implies computations on central frequencies (frequencies are not re-used at the border between two adjacent bands) and that the power for each frequency depends on the values of the frequencies.

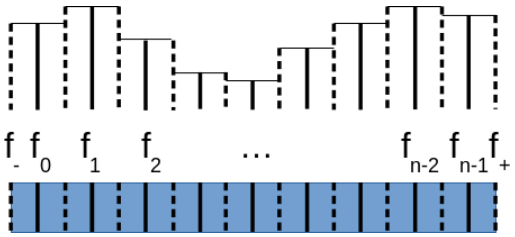

Figure 6.14: "rectangles-type" spectral sampling

"trapezes-type" integration

For a "trapezes-type" integration the band is sampled into $n+1$ frequencies, $\{f_0, f_1, \dots f_n\}$, with $f_- = f_0 < f_1 < \dots < f_{n-1} < f_n = f_+$, as illustrated on figure 6.15. The integration is performed by linearly interpolating the square of the electric field between E_i^2 and E_{i+1}^2 between the frequencies f_i and f_{i+1}. Hence on this interval:

$$E^2 = \frac{1}{f_{i+1} - f_i}\int_{f_i}^{f_{i+1}} \left(\frac{f_{i+1} - f}{f_{i+1} - f_i}E_i^2 + \frac{f - f_i}{f_{i+1} - f_i}E_{i+1}^2\right) df = \frac{1}{2}(E_i^2 + E_{i+1}^2) \tag{6.7}$$

As a consequence the power on each of the intervals is independent from the width of the intervals and equals to:

$$P_0 = \frac{1}{2}\frac{P}{n}\ ,\ P_i = \frac{P}{n} \text{ for } i \in \{1, 2, \dots n-1\}\ ,\ P_n = \frac{1}{2}\frac{P}{n} \tag{6.8}$$

And:

$$\sum_{i=0}^{n} P_i = P \text{ and we compute } E^2 = \sum_{i=0}^{n-1} E_i^2 \tag{6.9}$$

The pro of this method is obviously the independence from the width of the intervals. Nevertheless there is a different weight between band inner frequencies and outer frequencies. With a coarse sampling this difference of weighting is not justified.

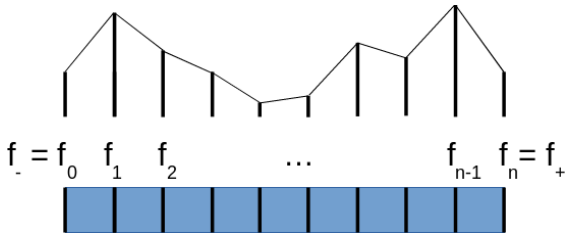

Figure 6.15: "trapezes-like" spectral sampling

"comb-like" integration

For a "comb-like" integration we use the same spectral sampling as for trapezes, i.e. $n+1$ frequencies $\{f_0, f_1, \ldots f_n\}$, width $f_- = f_0 < f_1 < \ldots < f_{n-1} < f_n = f_+$, as illustrated on figure 6.16. But now each frequency is given the same power. Hence:

$$P_i = \frac{P}{n+1} \tag{6.10}$$

And:

$$\sum_{i=0}^{n} P_i = P \text{ and we compute } E^2 = \sum_{i=0}^{n-1} E_i^2 \tag{6.11}$$

this is the method used in MithraREM as it is simple and stable with sampling variation as shown later. This method is not far from a Monte-Carlo sampling.

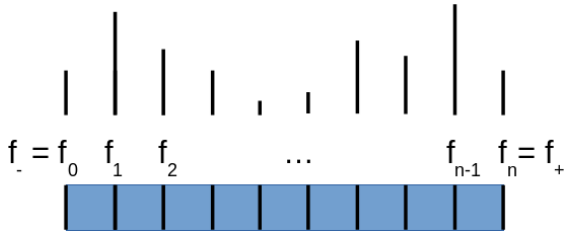

Figure 6.16: "comb-like" spectral sampling

6.8.2 Influence of spectral sampling

The number of frequencies used in a computation band has effects on the final result since interferences depend upon frequency. Nevertheless the convergence toward a stable solution is rather fast. On the contrary there are differences whether the computation is done in a more or less wide band.

Here we compare (for two virtual sites) the statistical parameters (average, maximum, RMS and median) for a ground computation and a frontages computation while varying sampling and bandwidth. Both sites have a single base station with three GSM 900 emitters on three azimuths.

num. freq.	step (MHz)	average	maximum	RMS	median
narrow band computation [925 MHz ; 935 MHz]					
3	3.33	0.276587	2.53112	0.437529	0.0894773
5	2	0.276603	2.53129	0.437191	0.0894857
7	1.43	0.276763	2.53165	0.437293	0.0894752
10	1	0.276743	2.53175	0.437351	0.0895045
15	0.67	0.276758	2.5318	0.437443	0.0895108
25	0.4	0.27677	2.53183	0.437519	0.089515
50	0.2	0.27678	2.53185	0.437575	0.0895129
wide band computation [925 MHz ; 960 MHz]					
8	4.38	0.276444	2.45942	0.434399	0.0894626
15	2.33	0.27649	2.45982	0.434369	0.0894354
25	1.4	0.27651	2.46307	0.434411	0.0894228
50	0.7	0.276523	2.46427	0.434476	0.0894375

Table 6.2: Spectral sampling influence - virtual site #1 - ground computation

num. freq.	step (MHz)	average	maximum	RMS	median
narrow band computation [925 MHz ; 935 MHz]					
3	3.33	0.358475	4.35791	0.64367	0.0899052
5	2	0.3585	4.36019	0.643478	0.0899264
7	1.43	0.3585	4.36095	0.643364	0.0899362
10	1	0.358501	4.36146	0.643334	0.0899264
15	0.67	0.358523	4.36117	0.643403	0.0899182
25	0.4	0.358523	4.36133	0.643397	0.089915
50	0.2	0.358519	4.36154	0.64338	0.0899134
wide band computation [925 MHz ; 960 MHz]					
8	4.38	0.358067	4.38213	0.642021	0.0899036
15	2.33	0.358106	4.38214	0.642121	0.0899068
25	1.4	0.35811	4.38215	0.642139	0.089915
50	0.7	0.358103	4.38215	0.642128	0.0899199

Table 6.3: Spectral sampling influence - virtual site #1 - frontages computation

num. freq.	step (MHz)	average	maximum	RMS	median
narrow band computation [925 MHz ; 935 MHz]					
3	3.33	0.272969	1.57231	0.365092	0.149873
5	2	0.27301	1.57281	0.364843	0.14982
7	1.43	0.273036	1.57298	0.36482	0.149667
10	1	0.273016	1.57309	0.364822	0.149682
15	0.67	0.273008	1.57317	0.364836	0.149563
25	0.4	0.273002	1.57323	0.364848	0.149595
50	0.2	0.272997	1.57327	0.364859	0.149627
wide band computation [925 MHz ; 960 MHz]					
8	4.38	0.273178	1.53722	0.362517	0.151804
15	2.33	0.273192	1.53879	0.362532	0.151835
25	1.4	0.273176	1.53944	0.362567	0.151812
50	0.7	0.273165	1.53991	0.362597	0.151748

Table 6.4: Spectral sampling influence - virtual site #2 - ground computation

num. freq.	step (MHz)	average	maximum	RMS	median
narrow band computation [925 MHz ; 935 MHz]					
3	3.33	0.318823	3.30451	0.543575	0.0979945
5	2	0.318832	3.30451	0.543103	0.097958
7	1.43	0.318825	3.30451	0.54313	0.097926
10	1	0.318838	3.30451	0.543152	0.0979352
15	0.67	0.318832	3.30451	0.543165	0.0979352
25	0.4	0.31883	3.30451	0.543176	0.0979397
50	0.2	0.318828	3.30451	0.543184	0.0979443
wide band computation [925 MHz ; 960 MHz]					
8	4.38	0.31854	3.30451	0.54267	0.0979717
15	2.33	0.318532	3.30451	0.54254	0.0979534
25	1.4	0.318521	3.30451	0.542563	0.0979489
50	0.7	0.318526	3.30451	0.542591	0.0979489

Table 6.5: Spectral sampling influence - virtual site #2 - frontages computation

6.9 Bug fixes

The CSTB2013 propagation model implementation also fixes minor bugs that existed in the CSTB2009 propagation model implementation.

Chapter 7

Description of propagation model CSTB2013-INDOOR

7.1 Introduction

The CSTB2013-INDOOR propagation model is an adaptation of CSTB2013 model, dedicated to indoor exposure just behind the exterior wall. As a matter of fact CSTB2013 propagation model (like CSTB2009 propagation model) is intended at computation of outdoor exposure (on the ground and on the frontages of buildings). For ground exposure, this model is identical to CSTB2013. In case of frontage receivers, this model deduces indoor exposure (just behind outer wall) from incident electric field with an incidence dependant loss factor (grazing incident waves are less penetrating).

7.2 Description

This propagation model is based upon indoor coverage model from outdoor emitter of COST 231 "Digital Mobile Radio towards Future Generation Systems". The formula is applied to compute the indoor electric field just behind the exterior wall. This is a heuristic model deduced from several measurements on real buildings. It it then statistically satisfying, since the local indoor behavior mostly depends on the (unknown) building structure.

7.2.1 Case of a free-field receiver

In case of a free-field receiver (ground receiver for instance), the computation is exactly the same as with CSTB2013 method. It is then outdoor exposure.

7.2.2 Case of a forward illumination

In case of a frontage receiver and a forward illumination (an incident wave coming from the front side of the frontage) the indoor electric field E_{int} for this incident wave is computed from the incident electric field incident E_{inc} with the formula:

$$20 \log E_{\text{int}} = 20 \log E_{\text{inc}} - W_{\text{E}} - (1 - \cos\theta)^2 W_{\text{GE}} \tag{7.1}$$

W_{E} is the normal incidence loss (in dB), θ is the incidence angle of the wave with the frontage (0° means normal incidence, 90° means grazing incidence) and W_{GE} the extra loss (in dB) for grazing incidence. W_{GE} is constant and equals 20 dB. W_{E} is deduced from the diffuse field loss factor W_{D} (depending on the frontage material in MithraREM) with the formula $W_{\text{E}} = W_{\text{D}} - 2.15$.

This 2.15 dB value is computed by simulating a diffuse electric field in frontage (with all incident directions as likely and with all incident electric field amplitude identical), with $W_{\mathrm{GE}} = 20$. We have then:

$$T^2_{\mathrm{diffuse}} = \frac{1}{\pi} \int_{\theta=0}^{\frac{\pi}{2}} \int_{\varphi=0}^{2\pi} T^2(\theta,\varphi)\, \cos\theta\, \sin\theta\, d\theta\, d\varphi = \int_{\theta=0}^{\frac{\pi}{2}} T^2(\theta)\, \sin 2\theta\, d\theta \tag{7.2}$$

With $W_{\mathrm{D}} = -20 \log T_{\mathrm{diffuse}}$ and $W_{\mathrm{E}} + (1-\cos\theta)^2 W_{\mathrm{GE}} = -20 \log T(\theta)$. Since W_{GE} is constant, equation 7.2 allows to link W_{E} and W_{D} (with numerical integration).

When the diffuse field loss W_{D} defined in MithraREM is lower than 2.15 dB, the value of W_{GE} is automatically adapted in order to have $W_{\mathrm{E}} = 0$ (hence the signal will not be amplified behind the wall, corresponding values are displayed in table 7.1). This leads to $W_{\mathrm{E}} = W_{\mathrm{GE}} = 0$ when $W_{\mathrm{D}} = 0$. It is logical since a zero diffuse field loss means void (no material) [1] and in this case there is no loss, whatever the incident angle is.

W_{D} (dB)	W_{E} (dB)	W_{GE} (dB)
0.00	0	0
0.16	0	1
0.32	0	2
0.46	0	3
0.60	0	4
0.73	0	5
0.86	0	6
0.98	0	7
1.09	0	8
1.20	0	9
1.31	0	10
1.41	0	11
1.50	0	12
1.60	0	13
1.69	0	14
1.77	0	15
1.85	0	16
1.93	0	17
2.01	0	18
2.08	0	19
2.15	0	20
> 2.15	$W_{\mathrm{D}} - 2.15$	20

Table 7.1: Values of W_{E} (normal incidence loss) and W_{GE} (extra grazing incidence loss) as a function of W_{D} (diffuse field loss) for CSTB2013-INDOOR method

7.2.3 Case of a backward illumination

In case of a frontage receiver and a backward illumination (an incident wave coming from backward, such as a diffraction effect by the building itself) the indoor electric field E_{int} for this incident wave is computed from the incident electric field E_{inc} with the formula:

$$20 \log E_{\mathrm{int}} = 20 \log E_{\mathrm{inc}} - W_{\mathrm{D}} \tag{7.3}$$

[1] This kind of transmission material allows to compute incident field.

7.3 Example of results

The overall effect of method CSTB2013-INDOOR lowers results compared to diffuse field loss factor (CSTB2013 method for the computation of outdoor exposure, diminished by the diffuse loss factor of the frontage material). That is to say that the average exposure will decrease. However as far as maximum exposure is concerned the result depends on the configuration. A normally illuminated frontage by an antenna will have a higher indoor electric field with CSTB2013-INDOOR method than with CSTB2013 method.

For instance for a virtual site with 25 locations, 36 emitters (GSM 900, GSM 1800, UMTS and LTE 800). W_{D} is 6 dB, but the analysis in dB is totally independant from this choice. For ≈40000 frontage receivers:

method	average	maximum	RMS
CSTB2013.1	0.52	6.72	0.94
CSTB2013-INDOOR	0.43	4.33	0.84

Results for each receiver obviously vary. We compare maximum electric field E computed with method CSTB2013 (outdoor electric field with diffuse loss depending on the material) and electric field E' computed with method CSTB2013-INDOOR. $\Delta = 20\log(E'/E)$ is the difference (in dB) between the two methods.

n	E	E'	Δ	n	E	E'	Δ	n	E	E'	Δ
1	6.72	1.72	-11.84	13	1.66	1.46	-1.12	25	0.93	0.98	+0.51
2	6.44	4.33	-3.44	14	1.10	1.01	-0.72	26	0.93	1.00	+0.69
3	1.10	1.27	+1.28	15	0.90	0.82	-0.83	27	0.69	0.67	-0.28
4	1.61	0.86	-5.42	16	1.10	1.25	+1.11	28	0.74	0.72	-0.28
5	1.34	1.24	-0.65	17	2.42	2.85	+1.41	29	1.41	1.41	0.00
6	0.79	0.91	+1.23	18	2.43	2.12	-1.19	30	0.98	0.98	0.00
7	0.72	0.82	+1.23	19	2.27	1.85	-1.80	31	0.90	0.63	-3.07
8	1.27	1.35	+0.54	20	2.83	2.62	-0.65	32	0.98	0.65	-3.55
9	0.40	0.37	-0.56	21	1.68	1.74	+0.33	33	1.17	1.00	-1.31
10	1.74	1.52	-1.13	22	1.57	1.16	-2.68	34	1.00	0.96	-0.35
11	0.81	0.76	-0.54	23	1.51	1.27	-1.50	35	0.96	0.77	-1.88
12	0.12	0.09	-2.24	24	2.39	2.07	-1.26	36	0.78	0.72	-0.65

The overall maxima decrease, but for some emitters they increase (lines in red). The maximum increases up to 1.4 dB on this example (the theoretical value being 2.15 dB minus the frontage reflection, for a perfect normal incidence). For instance, for a light concrete, the maximum increase is 1.44 dB.

It must be acknowledged that for incident angle lower than 45°, the diffuse loss factor is higher than the angle dependant loss factor.

The emitters where the maximum electric field is unchanged are the ones that do not generate forward illumination on the frontage.

Chapter 8

Description of propagation models CSTB2016 and CSTB2016-INDOOR

These models are an update of propagation models CSTB2013 and CSTB2013-INDOOR with an improvement of the higher exposure point lookup. In methods CSTB2013, those points where only searched with the main radiation lobe. Hence, when an antenna was in line of sight of a building, if the main lobe radiated above the building top, there was no maximum exposure lookup.

With CSTB2016 methods, this maximum exposure lookup is performed for every antenna in the line of sight of a reception column, and uses the complete vertical radiation pattern of the antenna. As a consequence, even if the main lobe is partially obstructed, of if the column is in a secondary lobe, there will still be a lookup of the maximum exposure point, enforcing a better stability of results.

Chapter 9

Description of propagation model HATA Ex

9.1 Introduction

The extended Hata is the one proposed by the European Telecommunication Office (ETO). This model is not detailed here, and its description can be found in ECC report 252 (`https://docdb.cept.org/download/1270`), section A17.3.1. It is suitable for a wide range of parameters (frequency range is 30MHz to 3GHz, it drops to free field propagation model at short distance).

9.2 Usage

This model has three different environment types : urbain, sub-urban, rural (propagation being favorable in urban environment).

The heights of the emitter and the receiver are considered relative to the lower altitude of the ground at both positions.

Chapter 10

Description of the HATA Ex + Fresnel propagation model

10.1 Introduction

This is a hybrid geometrical - heuristic propagation model, between first Fresnel ellipsoid clearance computation and extended Hata model. For a point-to-point link, the fraction of the ellipsoid that is obstructed by obstacles is computed, in ordrer to estimate the link loss. In case there is no direct visibility, the heuristic model is used. This hybrid approach correctly takes into account masking effects, and allows to reach lower frequencies. It is typically suitable for computations in the FM frequency band.

10.2 Principle

The Fresnel ellipsoid is a volume aound a radio link between an emitter A and a receiver B, whose outer boundary is defined with equation :

$$MA + MB = AB + n\,\frac{\lambda}{2} \tag{10.1}$$

Where λ is the wavelength, and for $n = 1$ we have the first Fresnel ellipsoid. If this ellipsoid is completly cleared (no obstacle such as a building is within its volume), there is a direct link (free field), without extra loss. If its partially obstructed (half), then the path loss is of 6 dB relative to free field loss, ...

In order to compute the ellipsoid clearance, it is discretized into a set of curved rays, with isovolume, as illustrated on figure 10.1. Those rays are also discretized into piecewise straight segments, and the clearance t (between 0 and 1) equals the ratio between the number of the cleared rays on the total number of rays.

If L is the path loss (in dB) given by the extended Hata model (positive as it is a loss), L_0 the free field path loss and t the clearance of the first Fresnel ellipsoid ($t = 1$ is the ellipsoid is totally cleared, $t = 0$ if it is fully obstructed), then hybrid path loss is given by :

$$K = \min\left(L_0 + 12(1-t), L\right) \tag{10.2}$$

$$L_{\text{hybrid}} = \begin{cases} K & \text{si } t > \frac{1}{2} \\ 2tK + (1-2t)L & \text{si } t \leq \frac{1}{2} \end{cases} \tag{10.3}$$

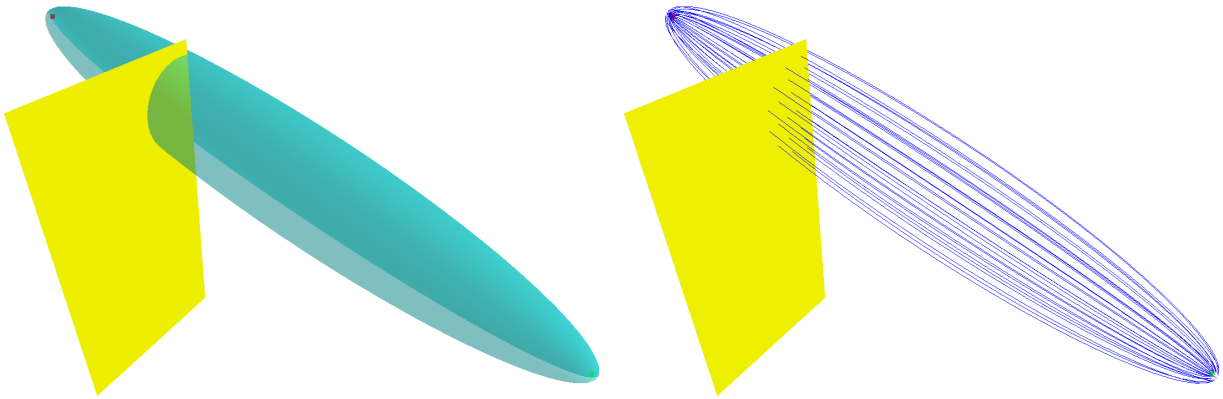

Figure 10.1: Fresnel ellipsoid : volume (left) and sampled with rays (right)

Part III

About the validation of the computations: methodology and examples of results for CSTB2009, CSTB2013 and HATA Ex + Fresnel propagation models

Chapter 11

Introduction

In general, science is based on hypotheses and approximations and any measure or numerical simulation of a physical phenomenon is necessarily flawed. Obtaining a strictly accurate measurement or simulation result is impossible and makes no sense.

An error is always related to something just or true, or considered as such. It is thus possible to speak of error only if one has available a value which can be considered as true.

In the case of the levels of electromagnetic fields radiated around radio antennas, as in many other physical domains, there is no true and absolute reference.

To estimate the electromagnetic field level around an antenna, two complementary approaches are used:

- metrology, it is possible to measure this quantity with a certain equipment, a protocol, a measurement method.
- numerical simulation, which is dependent on computational assumptions, more or less precise input data, calculated renderings and indicators, ...

For these two approaches, having no "true" reference value available, the physicist will use the more appropriate term for estimating uncertainty, Which translates the quality of the result obtained from an objective criticism of the means and parameters used to make the measurement or the numerical simulation.

CSTB engineers have developed wave propagation codes and laboratory or in situ measurement methods for more than 25 years. The validation of these methods, the estimation of the associated errors and uncertainties, is a continuous work carried out in parallel with the developments of the methods.

This document presents the methodology and some examples of results on the validation and estimation of the uncertainties of the calculation engine of the MithraREM software, Developed by the Lighting and Electromagnetic Division of the CSTB. This work, which is continuing with the evolutions of the methods, is based on numerous projects With different sources of financing (CSTB's own funds, public co-financing, contracts with private companies) and also take into account feedback from users of the MithraREM software.

Chapter 12

Methodology

Wanting to quantify the error associated with a simulation software by a precise value does not make sense. On the one hand there is no true value of the level of exposure, which can serve as a reference value and on the other hand the error also depends strongly on the use that is made of the software, beyond the methods that are implemented.

In particular, a measured value can not be considered as a true and absolute reference value.

Indeed, there are different measurement protocols, associated with separate equipment, and many parameters have to be taken into account to analyze the relevance and meaning of a measurement result: the frequency band, the detection, filtering and averaging parameters, the type of measured data (RMS value, maxhold), the temporal variability of the measured signal (variations related to traffic in mobile telephony or wifi for example), spatial averaging on the measurement points, ...

Thus, an electromagnetic field strength measurement result is also associated with an estimation of its uncertainty relative to the calibration drift of the equipment (probe, spectrum analyzer, decoder, ...), isotropy error, interpolation of antenna factors and cable losses, error on mismatch, influence of body in case of hand-held probe, the error related to the spatial integration of the data.

For example, uncertainties associated with measurements made under regulatory protocol in France [1] are estimated according to the laboratories between 4 and 6.5 dB on the electric field level (between 59 % and 111 % in V / m).

In the case of numerical simulations, the parameters to be taken into account in an estimation of uncertainties are the following:

- uncertainties related to radio input data: The sources of uncertainty are the emission characteristics of the antennas (power, gain, interpolation on the radiation pattern, cable losses), the geometrical characteristics of the antennas (positioning, height, azimuth).

- uncertainties related to the geometric model: The sources of uncertainty are the precision of the terrain and building model, the simplification of the geometry of facades and roofs, the sampling of calculation points (ground and frontage), the uncertainty on the materials used (reflection on the facades, indoor level), taking into account the spatial variation of the field level (Rice, Rayleigh laws).

- uncertainties related to the calculation method: The sources of uncertainty are related to the mathematical assumptions underlying the propagation equations and associated computational algorithms (in our case so-called asymptotic methods), parameters of the algorithms, the management and interpolation of the spectral calculation.

CSTB's expertise and know-how in relation to the MithraREM software are based on a relevant analysis of all these parameters in order to estimate at best the levels of electromagnetic exposure, but also the

[1] http://www.anfr.fr/fileadmin/mediatheque/documents/expace/Protocolofmeasurementinsitu_V331_mai_2011.pdf

uncertainties associated with each of these parameters. This is part of a global approach to validating methodologies developed at CSTB.

R&D at CSTB conditions the evolution of the MithraREM calculation model. These evolutions are validated one by one in comparison with other methods or with results of specific measurements. As described above, and as in any field of physics, a "digit to digit" comparison between simulation results and measurement result is not relevant. The methodology of validation and estimation of uncertainties of the CSTB is based on a qualitative approach, based on a statistical analysis of numerous complementary samples.

The following data are considered:

- other numerical or analytical methods: finite elements, moment method, free space model, propagation model for radio coverage, ...
- results of spectral measurements with a known and controlled transmitter,
- results of spectral measurements in real environment,
- results of broadband measurements (isotropic probe) in real environment.

For example, for the sources of error related to the calculation method, the uncertainties are estimated on the basis of comparison with results of numerical methods such as finite elements while statistically varying the identified parameters in a fixed interval and with an adapted distribution law (Monte-Carlo method). Different models are used: Simple canonical models in first approach, then test scenes representative of different urban environments.

Chapter 13

Validation examples

This section presents some examples of the assessment of MithraREM results. These results are not exhaustive and are given to illustrate the validation process used at CSTB.

13.1 Examples of numerical validations

13.1.1 Examples of canonical numerical validations

A numerical validation is useful to validate a local behavior of wave propagation, using a totally controlled environment (emitter, geometry, ...) and a numerical reference method such as the Finite Difference Time Domain (FDTD) method or the method of moments (MoM). For instance, the reference method can be applied to assess the reflection model used in MithraREM as illustrated on figure 13.1 (blue is the real part, green is the imaginary part of electric field).

Furthermore, numerical validations can be used to monitor local improvements of the MithraREM propagation model. On the example of figure 13.2 the diffraction scheme used in propagation model CSTB2013 improves the results, in terms of continuity and accuracy, for multiple close successive diffractions.

13.1.2 Example of numerical validation on complex cases

Numerical validation can also be used for more complex cases, involving multiple buildings, such as the curved surfaces on the example of figure 13.3.

Even if reference methods such as MoM solve the exact wave propagation equations, they also have their own limits (meshing, ...) and results must be analyzed with a critical mind.

13.2 Examples of comparisons with measurements

13.2.1 Example of comparisons with measurements for a controlled emitter

While numerical methods are mandatory to check local behaviors with complete control, comparisons with measurements are used to assess the global behavior of computations over large areas. In this case, we do not compare point-to-point electric field values. Instead, statistical information such as correlation and RMS error are exploited. Some results for publicly available path-losses in Munich and proprietary power measurements in Poitiers are displayed in table 13.1.

This example of results should not be considered with an absolute point of view (it would be easy to improve results by tuning specific parameters of the computation such as electromagnetic properties for instance), but with a relative point-of-view: switching from CSTB2009 to CSTB2013 propagation method improves the overall results, such as shown on figure 13.4.

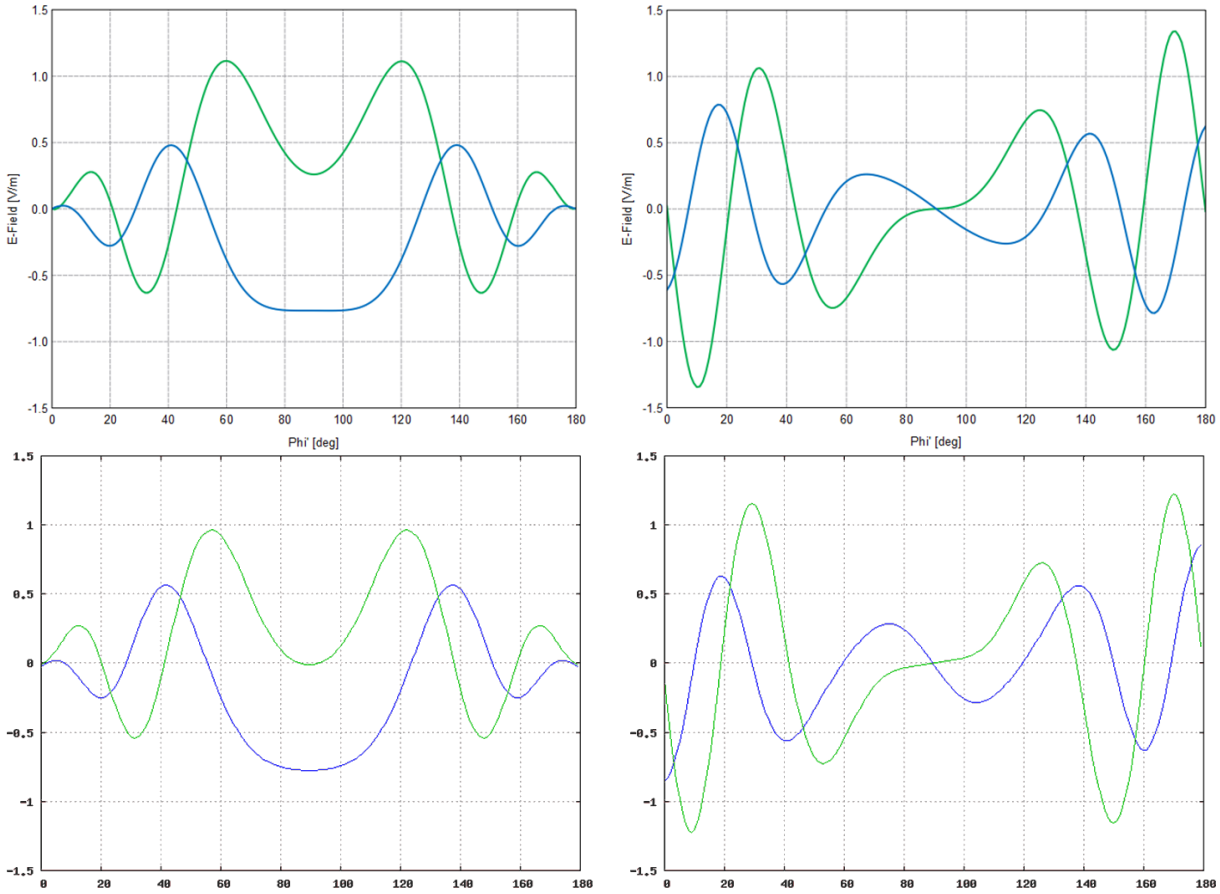

Figure 13.1: Reflection on impedant surfaces: MoM reference (top), MithraREM reflection model (bottom), sample #1 (left), sample #2 (right)

13.2.2 Other examples of comparisons with measurements for a controlled emitter

Other measurement campaigns with a controlled emitter on a building roof (CW at 2.3 GHz) have been conducted in october 2014, on six routes and two geographical sites. Figure 13.5 shows the emitter and the mobile acquisition station (GPS, fisheye camera and spectrum analyzer, all controlled by a laptop). Two examples of results from this campaign are presented here.

Results for route displayed on figure 13.6 are shown on figure 13.7. In this case correlation is 0.90 and RMS error is 2.5 dB.

Results for route displayed on figure 13.8 are shown on figure 13.9. In this case correlation is 0.82 and RMS error in 2.7 dB.

13.2.3 Example of comparisons with measurements on a real emitter

Comparisons of measurements on existing mobile telephony antennas and simulations are also performed. Results are highly dependant on the measurement protocol (spatial avergaging, time averaging, ...) and the subsequent equivalent process in the numerical simulation, and also on the real characteristics of emitters, that have to be precisely known.

For instance, for the case of figure 13.10 (CSTB measurements in Nantes, a single height per point,

route →	Munich #0		Munich #1		Munich #2		Poitiers	
method	corr.	error	corr.	error	corr.	error	corr.	error
CSTB2009	0.93	7.1 dB	0.80	7.3 dB	0.93	8.6 dB	0.87	5.5 dB
CSTB2013	0.94	6.6 dB	0.81	7.2 dB	0.94	8.4 dB	0.92	4.6 dB

Table 13.1: Comparisons with measurements for a controlled emiiter

quadratic averaging over a minute), the results for GSM 1800 are displayed on figure 13.11.

The example of result must be carefully analyzed since the characteristics of emitters are partially unknown and have been completed by generic data.

13.2.4 Example of comparaison with measurements for a FM emitter

We compare measurements and simulations for a given FM emitter, on a transmitting tower, in urban environment, as illustrated on figure 13.12.

The comparisons on this site (see figure 13.13) are carried with a free-field propagation model (green) and the hybrid HATA Ex + Fresnel propagation model (yellow), and compared to measurements (magenta). The measurements are close to free field results, being in an almost open area, except for masked areas, where free-field simulations are overestimatesrd. In those areas the hybrid model take correctly into account the progressive masking effect (mimicking the drop in level that is exhibited in measurements), and in areas where the first Fresnel ellipsoid in fully obstructed, the extended Hata model correctly estimates levels.

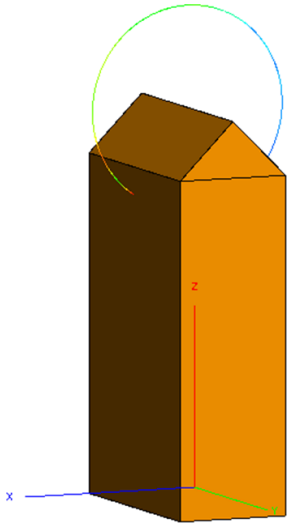

Diffraction by a slanted roof

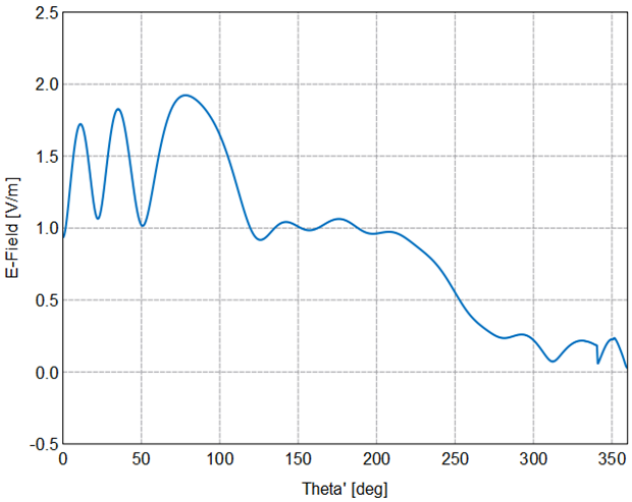

MoM reference computation

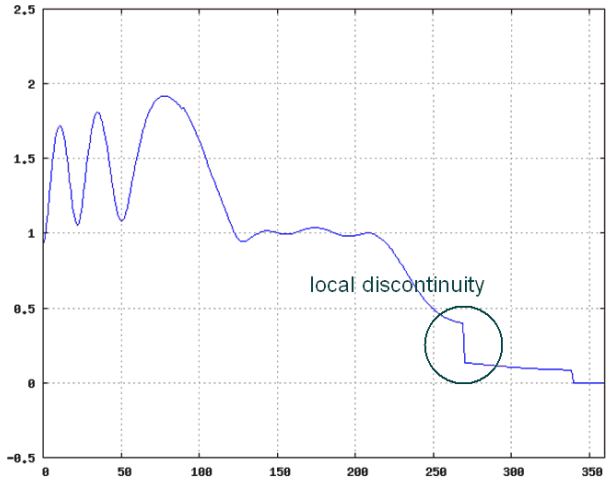

CSTB2009 diffraction scheme

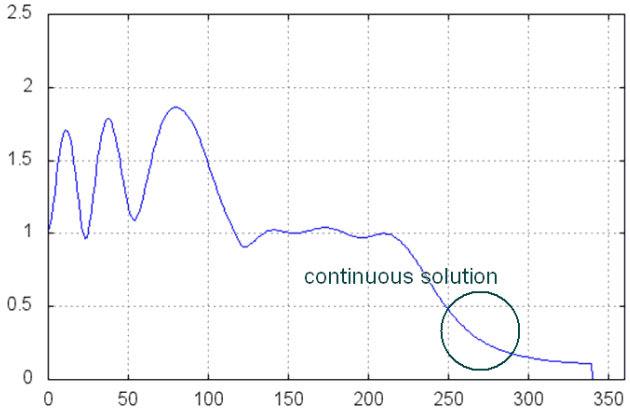

CSTB2013 diffraction scheme

Figure 13.2: MithraREM diffraction model validation

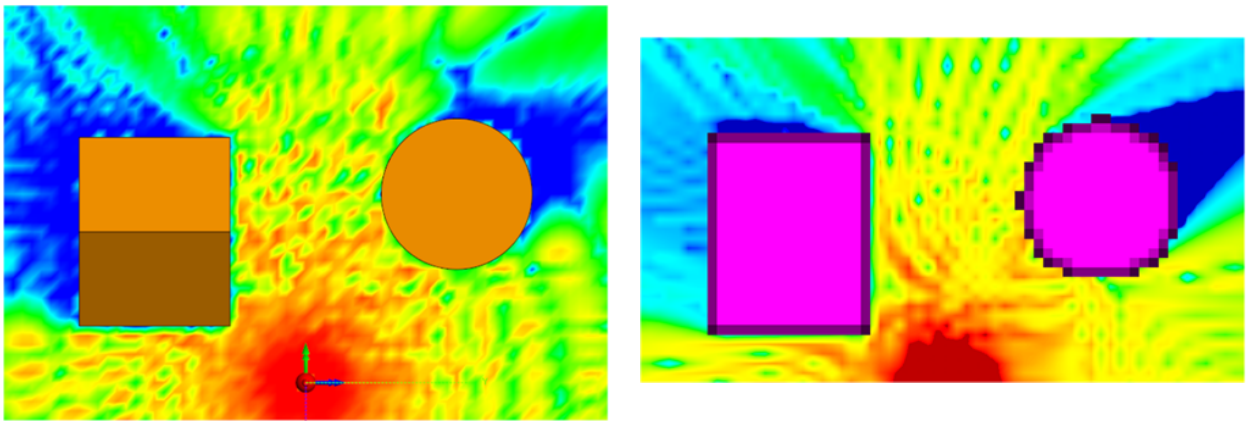

MoM computation MithraREM computation

Figure 13.3: MoM computation (left) and MithraREM computation (right) for a complex case

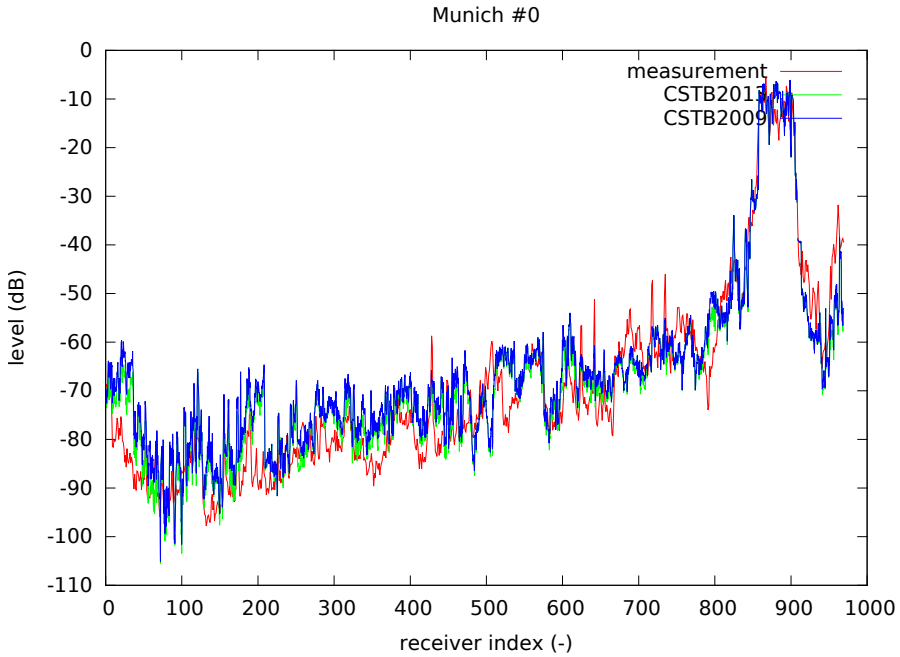

Figure 13.4: Comparison between measurement and simulation on a Munich route

Figure 13.5: Emitter and mobile acquisition station

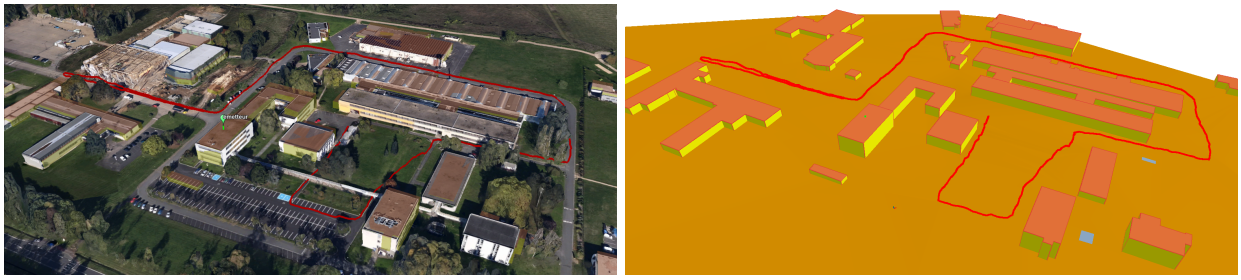

Figure 13.6: Poitiers Institude of Technology: Google Earth overview and computation model

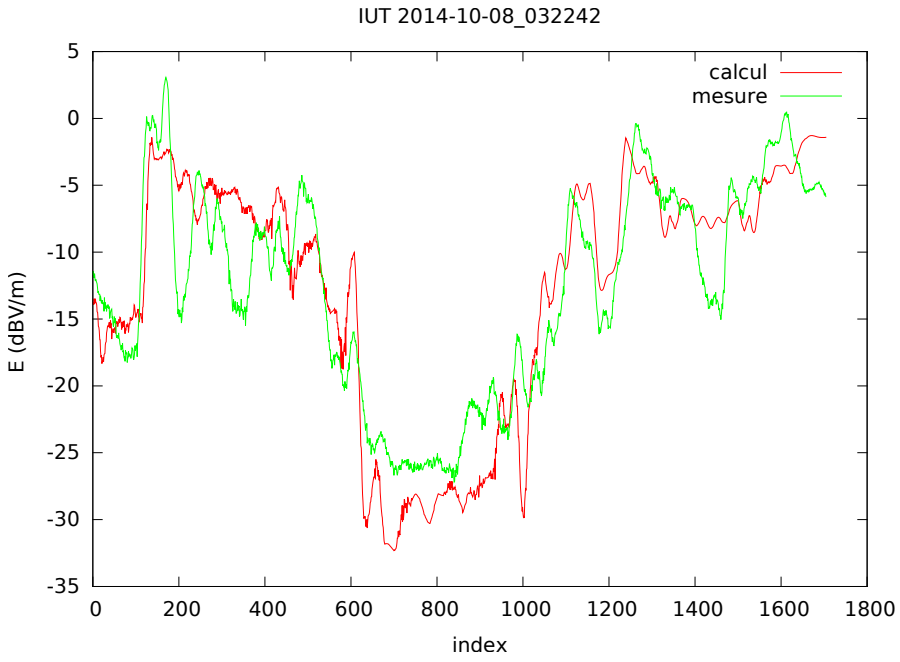

Figure 13.7: Comparison between measurements and simulations at Poitiers Institude of Technology

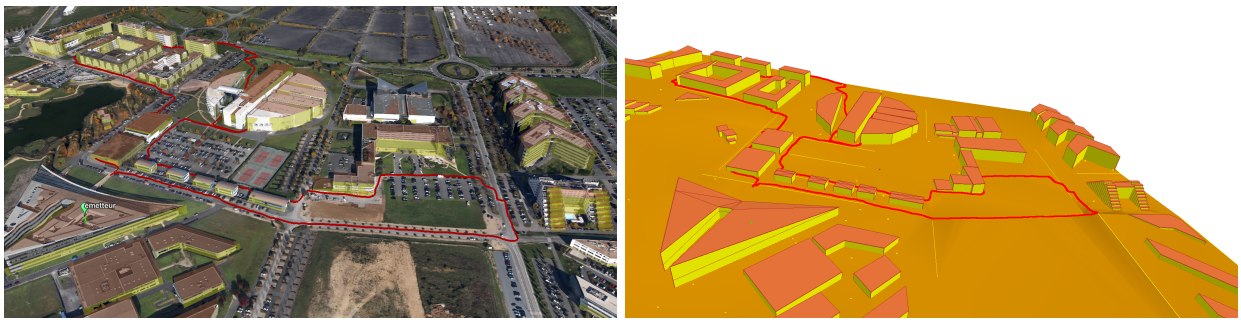

Figure 13.8: Futuroscope: Google Earth overview and computation model

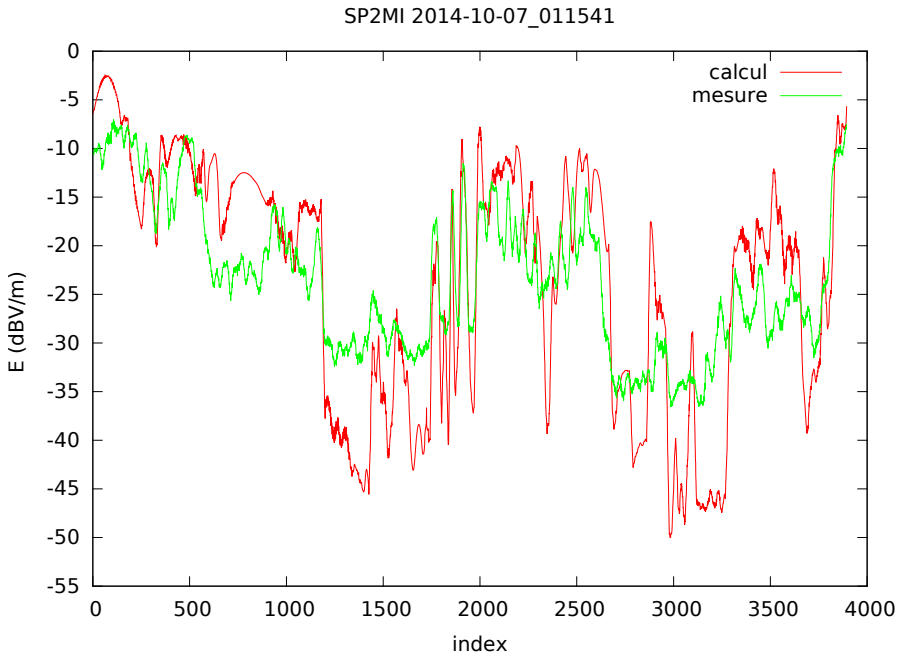

Figure 13.9: Comparison between measurements and simulations at Futuroscope

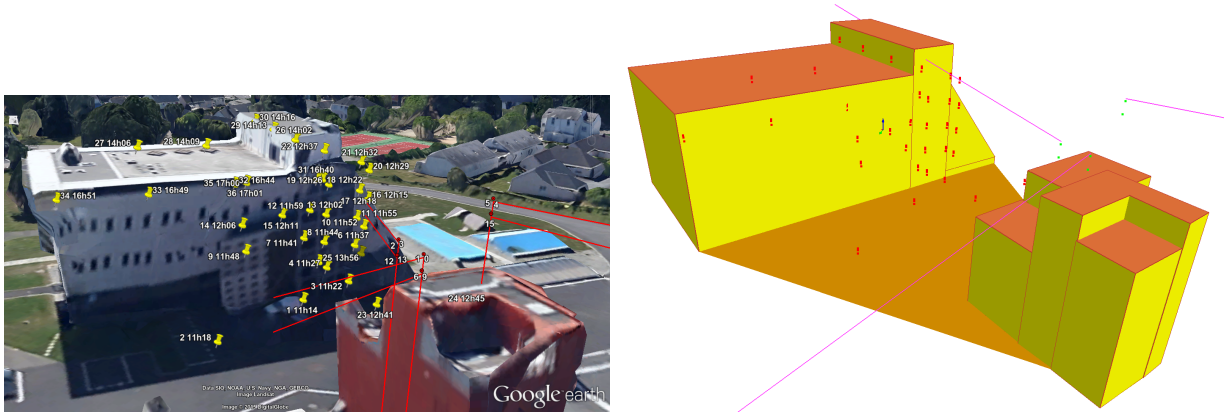

Figure 13.10: Measurements in the vicinity of a mobile telephony base station (Nantes, France) - site overview and measurement points (left), numerical model (right) - copyright CSTB

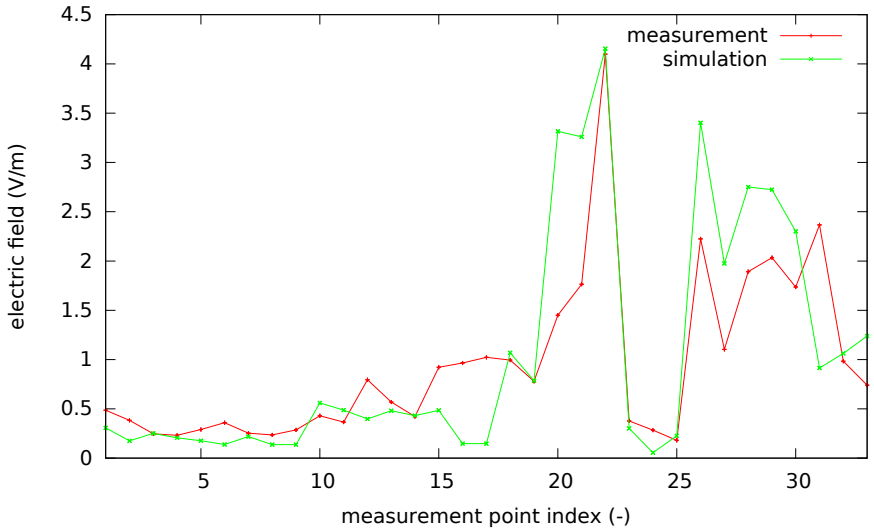

Figure 13.11: Example of comparison between measurements and simulations in Nantes, France (GSM 1800)

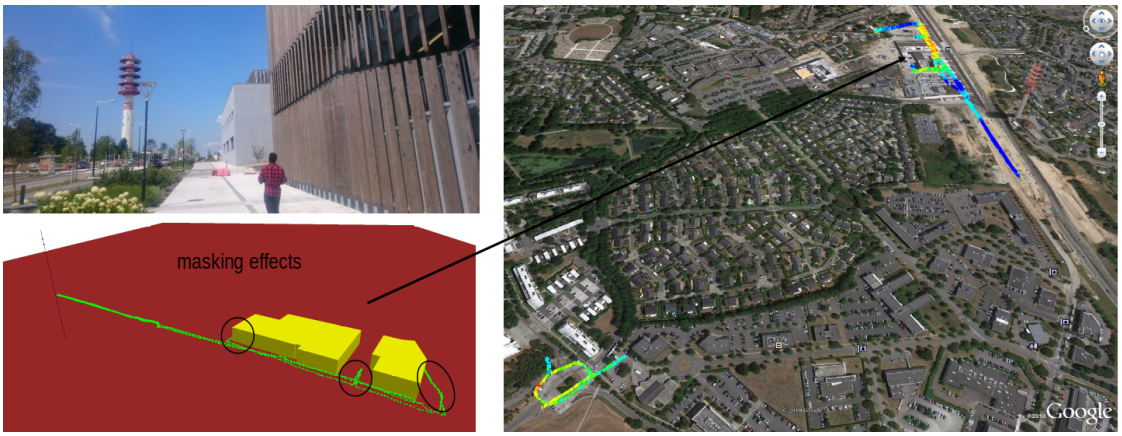

Figure 13.12: Measurements in the vicinity of a FM emitter on a tower : tower (top left), numerical model (bottom left) and measurements (right)

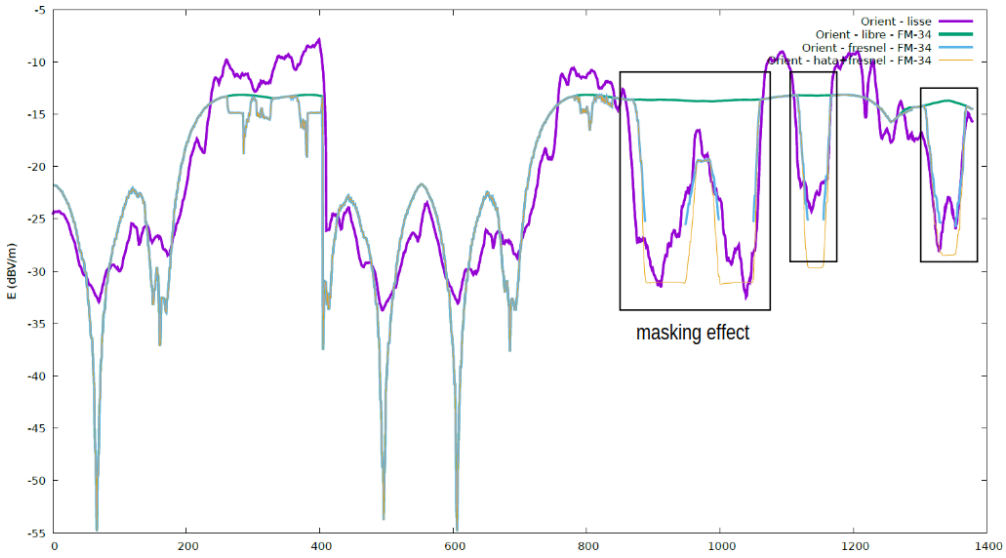

Figure 13.13: Comparison between measurement and simulation close to a FM emitter on a tower

13.2.5 Example of large scale comparison to measurements in the FM band

Measurements carried in the city of Bruxelles during a drivetest, for an FM emitter atop a building, were compared to simulation with three propagation models : free-field, extended Hata (HATA Ex) and HATA Ex + Fresnel. Table 13.2.5 displays averaged (signed) error E_1, averaged quadratic error E_2 and Pearson correlation p between measurement and simulation.

model	E_1 (dB)	E_2 (dB)	p
free-field	15.5	17.1	0.69
extended Hata	-4.3	7.4	0.80
hybrid	-1.3	6.3	0.83

The free-field model largely overestimates levels (as a lot of measurement points are not in line of sight of the antenna). On the other hand the extended Hata model underestimated levels (as it cannot determine visibility), and the hybrid model (HATA Ex + Fresnel) gives the better results, whether is be for averaged error, averaged quadratic error of correlation.

Chapter 14

Conclusion

Computation methods implemented in MithraREM software are developed and improved alongside a continuous body of work on results validation and uncertainties estimation. This is a multi-level work: comparisons with other numerical techniques and comparisons with measurement results (controlled emitter, real emitter). This results are analysed with statistics on an overall level and allow to both validate evolutions of the computation method and estimate uncertainties associated to parameters.

It is important to acknoledge that this document only focus on the computation method used by MithraREM. A global approach of validation, error and uncertainties must take into account all three successive levels:

- the computation method (as in this document),
- the software,
- the methodology.